**Figure 4** *(see previous page)*
**MDM2 induced the polyubiquitination of Vif *in vitro* and *in vivo*.** (A) GST-MDM2 induced the polyubiquitination of Vif *in vitro*. Bacterially expressed GST-Vif was subjected to *in vitro* ubiquitination assays. The reaction was performed in the presence or absence of E1, E2, GST-MDM2, and GST-Ubiquitin as indicated. Reactions were subjected to immunoblotting with anti-Vif mAb. Arrows indicate GST-ubiquitin-conjugated Vif. (B) Overexpressed MDM2 induced the polyubiquitination of Vif *in vivo*. HEK293T cells were cotransfected with expression vectors for MDM2 Wt and a ΔRF mutant together with expression vectors for Vif and His-Ubiquitin (His-Ub) as indicated. Cells were treated with MG132 for 6 hrs, and cell lysates were precipitated with Ni-NTA agarose beads followed by immunoblotting with the indicated Abs. Since Vif naturally bound to Ni-NTA agarose, we detected a Vif band itself (arrowhead), whereas no signal was detected in cells lacking Vif (lane 3). Arrows indicate His-Ub-conjugated Vif. Arrows with asterisk indicate Vif conjugated with endogenous ubiquitin. (C) Transduction of siRNA reduced cellular levels of endogenous MDM2 and polyubiquitination of Vif. HEK293T cells were cotransfected with expression vectors for MDM2 siRNA and control siRNA together with expression vectors for Vif and HA-Ubiquitin (HA-Ub). Cell lysates were immunoprecipitated with anti-Vif mAb followed by immunoblotting with the indicated Abs. Asterisk indicates immunoglobulin light chains from the immunoprecipitation.

sion of exogenous MDM2 efficiently induced polyubiquitination of Vif *in vivo*. Furthermore, the knock-down of endogenous MDM2 expression by introduction of MDM2-specific short interfering RNA (siRNA) resulted in a significant reduction in the amount of polyubiquitinated Vif, commensurate with the extent of reduced MDM2 expression (Fig. 4C). Collectively, these data indicated that MDM2 mediates polyubiquitination of Vif both *in vitro* and *in vivo*.

### *MDM2 negatively regulates HIV-1 replication in non-permissive cells through ubiqutination and degradation of Vif*

Next, we examined the effect of MDM2 on HIV-1 replication. In a single round infection assay (Fig. 5A), in the absence of A3G, viral replication was not affected by expression of MDM2 and/or Vif (lanes 1–6). In contrast, in the presence of A3G in a non-permissive cell setting, without the expression of MDM2, the wild type virus could replicate but the ΔVif virus could not, as previously reported (lanes 7 & 8) [3,8]. Co-expression of MDM2 reduced the cellular level of Vif (Fig. 5B, upper panel, lanes 5 & 11), resulting in the increased virion incorporation of A3G (Fig. 5B, 2nd lower panel, lane 11 as compared with lanes 7) and the greater suppression of viral replication (Fig. 5A, lane 11 as compared with lane 7).

We also tested the effect of MDM2 on HIV-1 replication in the presence of A3F. MDM2 suppressed viral replication in the presence of A3F, similar to results shown for A3G (Additional file 3). These data indicated that the MDM2-mediated Vif downregulation led to upregulated cellular A3G and A3F levels in producer cells, resulting in less infectious HIV-1 virions produced. Since MDM2 was previously reported to upregulate HIV-1 transcription by ubiquitination of Tat, we further examined HIV-1 replication in macrophages knocked down for MDM2 (Fig. 5C). We chose terminally differentiated macrophages as the target, because the knockdown of MDM2 is lethal for proliferating cells. HIV-1 replicated more efficiently in macrophages transfected with MDM2 siRNA than in control siRNA-transfected macrophages. These data indicated that MDM2 negatively regulated HIV-1 replication in non-permissive target cells through the ubiquitination and degradation of Vif.

To obtain further insights into the mechanisms why our MDM2 system did not induce the ubiquitination of A3G which was bound to Vif, we tested the expression levels and the binding affinity of A3G to Vif in transfected cells. Co-expression of MDM2 reduced the cellular levels of Vif and inversely increased the A3G levels in a dose dependent manner (Fig. 5D). Immunoprecipitation assays revealed that the co-expression of MDM2 blocked the binding of A3G to Vif in a dose dependent manner (Fig. 5E). These data suggest that the interaction between MDM2 and Vif precludes A3G from binding to Vif.

## Discussion

In this study, we report that MDM2 is a novel E3 ligase for HIV-1 Vif. MDM2 physically interacts with Vif and functions as an E3 ligase for Vif to induce its polyubiquitination and proteasomal degradation. Several E3 ligases including Cul5 [17], Nedd4, and AIP4 [18], have been reported to induce Vif ubiquitination, and the roles of Cul5 for Vif ubiquitination and degradation are especially well documented. Dang et al. have recently reported that Cul5 induces A3G degradation not by direct ubiquination of A3G but indirectly through Vif ubiqutination and that polyubiquitinated Vif might serve as a vehicle to transport A3G into proteasomes for degradation [23]. In this manuscript, we show that MDM2 only targets Vif for degradation but not A3G, although MDM2 and Cul5 both induce Vif ubiquitination (Additional file 2, part A). MDM2 reduced cellular Vif levels and inversely increased A3G levels (Fig. 5B &5D), unlike Cul5. One possible explanation is that the binding of MDM2 to Vif precluded A3G from binding Vif (Fig. 5E), whereas a Cul5-Vif complex

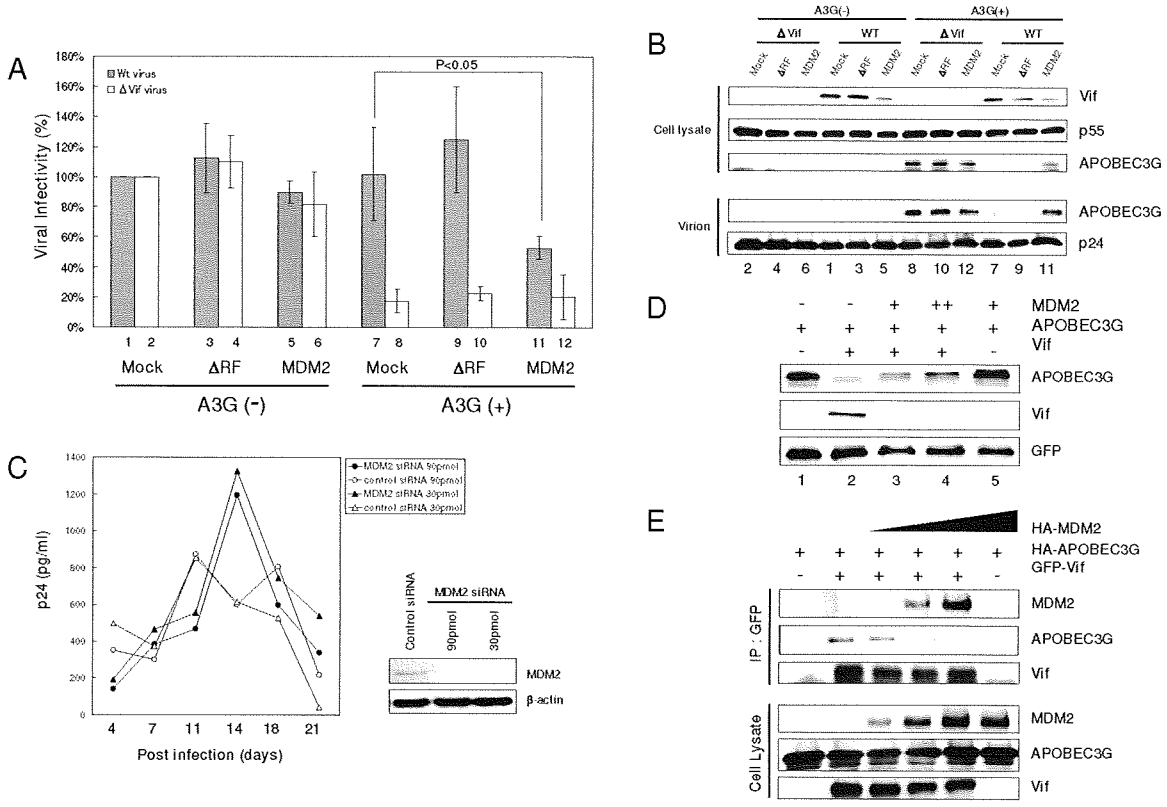


**Figure 5**

**MDM2 negatively regulated HIV-1 replication in non-permissive cells through the degradation of Vif.** (A) The overexpression of MDM2 inhibited HIV-1 replication in the presence of A3G. NL-43 Wt and ΔVif viruses were produced from HEK293T cells transfected with expression vectors for MDM2 Wt and a ΔRF mutant in the presence or absence of A3G. The viral infectivity was examined using M8166 cells. Values are presented as averages of more than 3 independent experiments. (B) MDM2 reduced cellular levels of Vif, resulting in more incorporation of A3G into HIV-1 virions. Immunoblotting for cell lysates (upper 3 panels) and precipitated virions (lower 2 panels) was performed with the indicated Abs. Lane numbers correspond to those in Fig. 4A. (C) HIV-1 replication in macrophages transfected with MDM2- and control-siRNA. MDM were transfected with MDM2- and control-siRNA and challenged with R5 HIV-$1_{JR-FL}$ (left panel). Cell lysates were subjected to immunoblotting with the indicated antibodies (right panels). (D) Coexpression of MDM2 reduced cellular levels of Vif and inversely increased A3G levels in a dose dependent manner. HEK293T cells were cotransfected with expression vectors for A3G, Vif, GFP, and MDM2 as indicated. Cell lysates were subjected to immunoblotting with the indicated Abs. (E) Immunoprecipitation assays revealed that the coexpression of MDM2 blocked the binding of A3G to Vif in a dose dependent manner. HEK293T cells were cotransfected with expression vectors for A3G, GFP-Vif, and MDM2 as indicated. Cell lysates were immunoprecipitated with anti-GFP mAb followed by immunoblotting with the indicated Abs.

can bind A3G to form a ternary complex. MDM2 binds the N-terminal region of Vif which does not overlap with, but is close to the A3G/A3F binding domain [25]. This binding might affect the interaction of Vif with A3G and/or A3F. Furthermore, the evidence that an MDM2 ΔRF mutant failed to protect A3G indicated that the ubiquitination and degradation of Vif is necessary to protect A3G and A3F from Vif. These findings suggest that different E3 ligases might play different roles in Vif ubiquitination. Further studies on the different roles of Vif ubiquitination by different E3 ligases and their virological significance should be investigated.

We demonstrate that MDM2 negatively regulated HIV-1 replication through Vif degradation. Through the degradation of target proteins (p53, pRB, etc), MDM2 can exert profound physiological effects on the regulation of cell cycle, cell proliferation, DNA repairs and other processes. To our knowledge, this is the first report to show that MDM2 plays an important role in viral replication

through the degradation of viral proteins. Recently, MDM2 was also reported to ubiquitinate HIV-1 Tat protein and activate its transcriptional activity in a non-proteolytic manner [26]. Our experiment using MDM2 knockdown macrophages showed that HIV-1 replication in these macrophages was more efficient than in control siRNA-transfected macrophages. These data are consistent with MDM2 negatively regulateing HIV-1 replication through Vif ubiquitination (Fig. 5C). However, the replication efficiency of HIV-1 in MDM2 knockdown macrophages was only 2-fold higher and was slower than in control siRNA-transfected macrophages. This suggests the possibilities that the ubiquitination of Tat might work as a positive regulatory factor at an earlier phase of infection and that MDM2 might be involved in both positive and negative regulation of HIV-1 replication at different stages. Further studies on the detailed effect of MDM2 on HIV-1 replication are needed.

We also demonstrated that Vif can bind MDM2 directly. We also mapped the interaction domain of MDM2 with Vif to amino acids 168–320 which is located in its central acidic and Zn finger domains. This central domain is different from the primary p53-binding site of MDM2 which is located in its N-terminal region; however, this central deomain was recently reported as a second p53-binding site and was shown to be important for the regulation of p53 stability [27-30] (Fig. 2B &2C). Interestingly, several proteins including p300, $p14^{ARF}$, and pRB bind to the central domain of MDM2 and regulate the stability and function of p53 via MDM2 [28,31]. Thus, it is possible that Vif might affect the stability and function of p53. Indeed, we confirmed that Vif can stabilize p53 (*Izumi et al., unpublished data*), which could explain why the effect of MDM2 on p53 degradation was weaker than that on Vif as shown in Fig. 1A. A further study is under way to elucidate this new function of Vif (*Izumi et al., HIV-1 Vif induces G2 cell cycle arrest via the p53 pathway, unpublished*).

Finally, expanding evidence suggests that the ubiquitination system plays important roles in many aspects of HIV-1 replication including the degradation of A3G by Vif [9-11], the degradation of CD4 by Vpu [32], HIV-1 viral budding [33], Tat-mediated transactivation [26], and Vpr-induced G2 cell cycle arrest [34,35]. The functional linkage between Vif and MDM2 also suggests that ubiquitin processes such as the A3G/Vif interplay is highly complex. It is obvious that HIV-1 replication in target CD4+ T cells is strongly affected by the interplay of these proteins. From the viral point of view, this interplay might give an advantage to HIV-1 replication. One possibility is that MDM2 regulates cellular Vif levels appropriately, such as not to affect viral replication [36] but just enough to antagonize A3G. Recent studies suggest that the G-to-A mutations induced by A3G may not be the mechanism by which A3G restricts or controls viral replication [37] and that a partially effective Vif inhibitor may actually accelerate the evolution of drug resistance and immune escape [38]. The inhibitory activity of MDM2 toward Vif could be partially effective and therefore could lead to viral evolution of drug resistance and immune escape. More recently, Nathans et al. have reported a small molecule that specifically antagonizes Vif function and inhibits viral replication by targeting the A3G/Vif axis. This compound enhances Vif degradation only in the presence of A3G, but does not induce A3G degradation and rather stabilizes A3G. They suggested the possibility of a new proteolytic enzyme for Vif degradation and that their new compound interferes with Vif interaction with a host protein in a Vif-A3G-host protein complex, thereby making Vif less stable. The precise biological significance of this Vif-A3G-host protein complex requires future elucidation. Nevertheless, modification or intervention of such Vif-A3G-host protein interplay could lead to the development of new therapeutic strategies for HIV-1 infection.

## Conclusion

MDM2 is a novel E3 ligase for Vif which induces the polyubiquitination and degradation of Vif to negatively regulate HIV-1 replication.

## Methods

### *Plasmid constructs*

Expression vectors for hemagglutinin (HA)- or FLAG-tagged MDM2, pCMV4/HA-MDM2 or pCMV4/FLAG-MDM2, and their mutants were constructed as previously described [19]. An expression vector for HA-tagged human APOBEC3G, pcDNA3/HA-hA3G [39], and HIV-1 reporter plasmids, pNL43/Δenv-Luc (WT) and pNL43/ΔenvΔvif-Luc (ΔVif) [8], were constructed as previously described. Expression vectors for FLAG-tagged Parkin and Cul5 (pcDNA3/FLAG-Parkin and pcDNA3/FLAG-Cul5, respectively) were constructed by the PCR method. Complementary DNA for HIV-1 Vif was also cloned into pDON-AI (TAKARA BIO INC.) and pDON/EGFP for expression of Vif and EGFP-fused Vif (EGFP-Vif). The subgenomic expression vector pNL-A1, which expresses all HIV-1 proteins except for *gag* and *pol* products, and its mutants expressing Vif deletion mutants were kind gifts from Dr. K. Strebel [22].

### *Co-immunoprecipitation assays*

We performed an immunoprecipitation assay for protein-protein interaction *in vivo*, as described previously [8]. HEK293T cells were cotransfected with pCMV4/HA-MDM2 and pNL-A1 by the calcium phosphate method. Two days after transfection, cells were lysed in lysis buffer (25 mM HEPES pH7.4/150 mM NaCl/1 mM $MgCl_2$/0.5% TritonX-100/10% Glycerol) and complexes were immunoprecipitated with anti-MDM2 monoclonal antibody

(mAb) (SMP-14, Santa Cruz Biotechnology, Inc., Santa Cruz, CA and Ab-1, Calbiochem, EMD Biosciences, Inc, Darmstadt, Germany) and Protein A-Sepharose beads (Amersham Biosciences Corp.) at 4°C. The beads were washed with RIPA buffer (50 mM Tris-HCl pH8.0/150 mM NaCl/1% Triton-X 100/0.1% SDS/0.1% DOC) and analyzed by immunoblotting with anti-Vif mAb (#319) (A kind gift from Dr. M. Malim through the AIDS Research and Reference Reagent Program) [40] or anti-HA mAb (12CA5). To map the regions of MDM2 necessary for binding to Vif, HEK293T cells were cotransfected with expression vectors for a series of MDM2 deletion mutants together with pNL-A1. Complexes were immunoprecipitated with anti-HA mAb and analyzed by immunoblotting with anti-Vif mAb. To map the regions of Vif necessary for binding to MDM2, HEK293T cells were cotransfected with expression vectors for a series of Vif deletion mutants together with pCMV4/HA-MDM2. Complexes were immunoprecipitated with anti-Vif mAb and analyzed by immunoblotting with anti-MDM2 mAb. In all these experiments, transfected cells were treated with MG132 for 6 hrs prior to harvesting in order to stabilize both Vif and MDM2; otherwise we could not detect the expression of MDM2 because of its rapid degradation, as seen in Fig. 1A.

#### *In vitro and in vivo ubiquitination assays*

*In vitro* ubiquitination assays were carried out in ubiquitin reaction buffer (50 mM Tris-HCl/2 mM ATP/5 mM $MgCl_2$/2 μM DTT) with E1(200 ng), E2(Ubc5c)(150 ng), and GST-tagged ubiquitin (GST-Ub) (10 μg) as described previously [13]. MDM2 and Vif were expressed as GST-fusion proteins in Escherichia coli strain DH5α and BL21, respectively. The reactions were incubated at 30°C for 90 min. The samples were subjected to immunoblotting with anti-Vif mAb to detect GST-ubiquitin conjugated Vif.

For *in vivo* ubiquitination assays, HEK 293T cells were cotransfected with plasmids expressing Vif, FLAG-MDM2 or its mutants, and His-tagged ubiquitin (His-Ub) as indicated. Cells were treated with 10 μM MG132 for 6 hrs prior to harvesting. Forty-eight hours post transfection, cell lysates were affinity-purified with Ni-NTA-agarose beads (Invitrogen corporation, Carlsbad, CA) and analyzed by immunoblotting with anti-Vif mAb.

For production of RNAi within the cells, we used the pSuper vector as described previously [19]. pSuper-MDM2-1 contained the 19 nt derived from the *mdm2* cDNA (nt 404–422) as the target sequence. Double-stranded RNA containing scrambled 19 nt was used as a control. HEK293T cells were transfected with pSuper plasmids together with plasmids expressing Vif and HA-Ub. Cell lysates were immunoprecipitated with anti-Vif mAb followed by immunoblottimg with anti-HA mAb.

#### *Single round infection assays with HIV-1 luciferase reporter virus*

Luciferase reporter viruses with or without Vif were prepared by cotransfection of pNL43/Δenv-Luc (Wt) or pNL43/ΔenvΔvif-Luc (ΔVif) plus pVSV-G together with a mock vector or an expression vector for MDM2 or a mutant in the presence or absence of pcDNA3/hA3G by calcium phosphate as previously described [8]. The reporter viruses were adjusted according to p24 values and used to infect M8166 target cells. Productive infection was measured by luciferase activity and values were presented as percent infectivity relative to the value of each virus without the expression of hA3G.

#### *Knockdown of MDM2 in macrophages and replication assays*

Monocyte-derived macrophages (MDM) were cultured for 7 days from CD14+ monocytes isolated from the peripheral blood of an HIV-1-negative healthy individual. Electroporation with Stealth Select RNAi for MDM2 or Control (Invitrogen Corporation) was performed using the Nucleofector machine (Amaxa Inc., Gaithersburg, MD) according to the manufacturer's instructions. Twenty four hours after transfection, MDM were challenged with R5 HIV-$1_{JR-FL}$ at multiplicity of infection of 0.1 at 37°C for 3 hrs. The cells were cultured from day 4 to 21 after infection, and the concentration of p24 antigen in the supernatant was measured with an HIV-1 p24 antigen enzyme-linked immunosorbent assay [ELISA] kit (ZeptMetrix, Buffalo, NY).

## Competing interests

The authors declare that they have no competing interests.

## Authors' contributions

TI. designed research, performed research, contributed vital new reagents, analyzed data, and wrote the paper. ATK designed research, analyzed data, wrote the paper, and organized the research. KS, KIo, and MM prepared the materials and performed a part of the research. KIwai, HK, TS, MT, SI., and HA contributed vital new reagents. YK contributed vital new reagents, performed a part of the research, and analyzed the data. HH, KItoh, and JF designed the research, contributed vital new reagents, and analyzed the data. TU analyzed the data, drafted the paper, and organized the research.

## Additional material

### Additional file 1

*Supplementary figure 1 – the stability of Vif protein in p53-/- MEF and p53-/-MDM2-/- MEF cells. MEF cells were transfected with pDON/Vif or pcDNA3/HA-A3G. Twenty-two hours after transfection, the cells were treated with cycloheximide (CHX) for the indicated times, and cell lysates were subjected to immunoblotting with the indicated Abs.*
Click here for file
[http://www.biomedcentral.com/content/supplementary/1742-4690-6-1-S1.pdf]

### Additional file 2

*Supplementary figure 2 – immunopurified MDM2 induced the polyubiquitination of Vif* in vitro. *(A) MDM2 as well as Cul5 induced the polyubiquitination of Vif. HEK293T cells were transfected with expression vectors for His-MDM2 and His-Cul5. His-tagged proteins were purified using Ni-NTA agarose and subjected to* in vitro *ubiquitination assays as described in a legend to Fig. 4A. Reactions were subjected to immunoblotting with anti-Vif Ab. Arrows indicate GST-Ub-conjugated Vif. Asterisks indicate non-specific bands associated with GST-Vif protein recognized by anti-Vif Ab, as they are seen in lanes 1 and 3. (B) MDM2 induced the polyubiquitination of Vif Wt but not that of Δ22 that was defective for binding MDM2. Filled asterisks indicate non-specific bands associated with GST-Vif protein, while white asterisks indicate those associated with GST-Vif Δ22.*
Click here for file
[http://www.biomedcentral.com/content/supplementary/1742-4690-6-1-S2.pdf]

### Additional file 3

*Supplementary figure 3 – the overexpression of MDM2 inhibited HIV-1 replication in the presence of A3F. Single round infection assays were performed in the presence or absence of A3F as described in a legend to Fig. 5A. Values are presented as averages of more than 3 independent experiments.*
Click here for file
[http://www.biomedcentral.com/content/supplementary/1742-4690-6-1-S3.pdf]

## Acknowledgements

We thank Drs. K. Strebel for the pNL-A1 plasmid and its derivative mutants, D. P. Lane for $p53^{-/-}MDM2^{-/-}$ DKO-MEF, and M. Malim for the anti-Vif mAb (#319) through the AIDS Research and Reference Reagent Program, Division of AIDS, NIAID, NIH. This study was partly supported by grants-in-aid from the Ministry of Education, Culture, Sports, Science, and Technology, from the Ministry of Health, Labour and Welfare, Japan, from the Naito Foundation, and from Mitsubishi Pharma Research Foundation.

## References

1. Goff SP: **Retrovirus restriction factors.** *Mol Cell* 2004, **16**:849-859.
2. Towers GJ: **The control of viral infection by tripartite motif proteins and cyclophilin A.** *Retrovirology* 2007, **4**:40.
3. Sheehy AM, Gaddis NC, Choi JD, Malim MH: **Isolation of a human gene that inhibits HIV-1 infection and is suppressed by the viral Vif protein.** *Nature* 2002, **418**:646-650.
4. Goila-Gaur R, Strebel K: **HIV-1 Vif, APOBEC, and intrinsic immunity.** *Retrovirology* 2008, **5**:51.
5. Mangeat B, Turelli P, Caron G, Friedli M, Perrin L, Trono D: **Broad antiretroviral defence by human APOBEC3G through lethal editing of nascent reverse transcripts.** *Nature* 2003, **424**:99-103.
6. Harris RS, Bishop KN, Sheehy AM, Craig HM, Petersen-Mahrt SK, Watt IN, Neuberger MS, Malim MH: **DNA deamination mediates innate immunity to retroviral infection.** *Cell* 2003, **113**:803-809.
7. Zhang H, Yang B, Pomerantz RJ, Zhang C, Arunachalam SC, Gao L: **The cytidine deaminase CEM15 induces hypermutation in newly synthesized HIV-1 DNA.** *Nature* 2003, **424**:94-98.
8. Shindo K, Takaori-Kondo A, Kobayashi M, Abudu A, Fukunaga K, Uchiyama T: **The enzymatic activity of CEM15/Apobec-3G is essential for the regulation of the infectivity of HIV-1 virion but not a sole determinant of its antiviral activity.** *J Biol Chem* 2003, **278**:44412-44416.
9. Marin M, Rose KM, Kozak SL, Kabat D: **HIV-1 Vif protein binds the editing enzyme APOBEC3G and induces its degradation.** *Nat Med* 2003, **9**:1398-1403.
10. Sheehy AM, Gaddis NC, Malim MH: **The antiretroviral enzyme APOBEC3G is degraded by the proteasome in response to HIV-1 Vif.** *Nat Med* 2003, **9**:1404-1407.
11. Stopak K, de Noronha C, Yonemoto W, Greene WC: **HIV-1 Vif blocks the antiviral activity of APOBEC3G by impairing both its translation and intracellular stability.** *Mol Cell* 2003, **12**:591-601.
12. Yu X, Yu Y, Liu B, Luo K, Kong W, Mao P, Yu XF: **Induction of APOBEC3G ubiquitination and degradation by an HIV-1 Vif-Cul5-SCF complex.** *Science* 2003, **302**:1056-1060.
13. Kobayashi M, Takaori-Kondo A, Miyauchi Y, Iwai K, Uchiyama T: **Ubiquitination of APOBEC3G by an HIV-1 Vif-Cullin5-Elongin B-Elongin C Complex Is Essential for Vif Function.** *J Biol Chem* 2005, **280**:18573-18578.
14. Zheng Y-H, Irwin D, Kurosu T, Tokunaga K, Sata T, Peterlin BM: **Human APOBEC3F Is Another Host Factor That Blocks Human Immunodeficiency Virus Type 1 Replication.** *J Virol* 2004, **78**:6073-6076.
15. Shirakawa K, Takaori-Kondo A, Kobayashi M, Tomonaga M, Izumi T, Fukunaga K, Sasada A, Abudu A, Miyauchi Y, Akari H: **Ubiquitination of APOBEC3 proteins by the Vif-Cullin5-ElonginB-ElonginC complex.** *Virology* 2006, **344**:263-266.
16. Fujita M, Akari H, Sakurai A, Yoshida A, Chiba T, Tanaka K, Strebel K, Adachi A: **Expression of HIV-1 accessory protein Vif is controlled uniquely to be low and optimal by proteasome degradation.** *Microbes Infect* 2004, **6**:791-798.
17. Mehle A, Goncalves J, Santa-Marta M, McPike M, Gabuzda D: **Phosphorylation of a novel SOCS-box regulates assembly of the HIV-1 Vif-Cul5 complex that promotes APOBEC3G degradation.** *Genes Dev* 2004, **18**:2861-2866.
18. Dussart S, Courcoul M, Bessou G, Douaisi M, Duverger Y, Vigne R, Decroly E: **The Vif protein of human immunodeficiency virus type 1 is posttranslationally modified by ubiquitin.** *Biochem Biophys Res Commun* 2004, **315**:66-72.
19. Higashitsuji H, Itoh K, Sakurai T, Nagao T, Sumitomo Y, Masuda T, Dawson S, Shimada Y, Mayer RJ, Fujita J: **The oncoprotein gankyrin binds to MDM2/HDM2, enhancing ubiquitylation and degradation of p53.** *Cancer Cell* 2005, **8**:75-87.
20. Honda R, Tanaka H, Yasuda H: **Oncoprotein MDM2 is a ubiquitin ligase E3 for tumor suppressor p53.** *FEBS Lett* 1997, **420**:25-27.
21. Yu Y, Xiao Z, Ehrlich ES, Yu X, Yu X-F: **Selective assembly of HIV-1 Vif-Cul5-ElonginB-ElonginC E3 ubiquitin ligase complex through a novel SOCS box and upstream cysteines.** *Genes Dev* 2004, **18**:2867-2872.
22. Strebel K, Daugherty D, Clouse K, Cohen D, Folks T, Martin MA: **The HIV 'A' (sor) gene product is essential for virus infectivity.** *Nature* 1987, **328**:728-730.
23. Dang Y, Siew LM, Zheng YH: **APOBEC3G is degraded by the proteasomal pathway in a Vif-dependent manner without being polyubiquitylated.** *J Biol Chem* 2008, **283**:13124-13131.
24. Honda R, Yasuda H: **Activity of MDM2, a ubiquitin ligase, toward p53 or itself is dependent on the RING finger domain of the ligase.** *Oncogene* 2000, **19**:1473-1476.
25. He Z, Zhang W, Chen G, Xu R, Yu XF: **Characterization of conserved motifs in HIV-1 Vif required for APOBEC3G and APOBEC3F interaction.** *J Mol Biol* 2008, **381**:1000-1011.
26. Brès V, Kiernan RE, Linares LK, Chable-Bessia C, Plechakova O, Tréand C, Emiliani S, Peloponese JM, Jeang KT, Coux O, Scheffner M, Benkirane M: **A non-proteolytic role for ubiquitin in Tat-medi-**

**ated transactivation of the HIV-1 promoter.** *Nat Cell Biol* 2003, **5**:754-761.
27. Argentini M, Barboule N, Wasylyk B: **The contribution of the acidic domain of MDM2 to p53 and MDM2 stability.** *Oncogene* 2001, **20**:1267-1275.
28. Iwakuma T, Lozano G: **MDM2, an introduction.** *Mol Cancer Res* 2003, **1**:993-1000.
29. Kawai H, Wiederschain D, Yuan ZM: **Critical contribution of the MDM2 acidic domain to p53 ubiquitination.** *Mol Cell Biol* 2003, **23**:4939-4947.
30. Meulmeester E, Frenk R, Stad R, de Graaf P, Marine JC, Vousden KH, Jochemsen AG: **Critical role for a central part of Mdm2 in the ubiquitylation of p53.** *Mol Cell Biol* 2003, **23**:4929-4938.
31. Ganguli G, Wasylyk B: **p53-independent functions of MDM2.** *Mol Cancer Res* 2003, **1**:1027-1035.
32. Margottin F, Bour SP, Durand H, Selig L, Benichou S, Richard V, Thomas D, Strebel K, Benarous R: **A novel human WD protein, h-beta TrCp, that interacts with HIV-1 Vpu connects CD4 to the ER degradation pathway through an F-box motif.** *Mol Cell* 1998, **1**:565-574.
33. Freed EO: **Viral late domains.** *J Virol* 2002, **76**:4679-4687.
34. Wen X, Duus KM, Friedrich TD, de Noronha CM: **The HIV1 protein Vpr acts to promote G2 cell cycle arrest by engaging a DDB1 and Cullin4A-containing ubiquitin ligase complex using VprBP/DCAF1 as an adaptor.** *J Biol Chem* 2007, **282**:27046-27057.
35. Schrofelbauer B, Hakata Y, Landau NR: **HIV-1 Vpr function is mediated by interaction with the damage-specific DNA-binding protein DDB1.** *Proc Natl Acad Sci USA* 2007, **104**:4130-4135.
36. Akari H, Fujita M, Kao S, Khan MA, Shehu-Xhilaga M, Adachi A, Strebel K: **High level expression of human immunodeficiency virus type-1 Vif inhibits viral infectivity by modulating proteolytic processing of the Gag precursor at the p2/nucleocapsid processing site.** *J Biol Chem* 2004, **279**:12355-12362.
37. Ulenga NK, Sarr AD, Hamel D, Sankale JL, Mboup S, Kanki PJ: **The level of APOBEC3G (hA3G)-related G-to-A mutations does not correlate with viral load in HIV type 1-infected individuals.** *AIDS Res Hum Retroviruses* 2008, **24**:1285-1290.
38. Pillai SK, Wong JK, Barbour JD: **Turning up the volume on mutational pressure: is more of a good thing always better? (A case study of HIV-1 Vif and APOBEC3).** *Retrovirology* 2008, **5**:26.
39. Kobayashi M, Takaori-Kondo A, Shindo K, Abudu A, Fukunaga K, Uchiyama T: **APOBEC3G Targets Specific Virus Species.** *J Virol* 2004, **78**:8238-8244.
40. Simon JH, Southerling TE, Peterson JC, Meyer BE, Malim MH: **Complementation of vif-defective human immunodeficiency virus type 1 by primate, but not nonprimate, lentivirus vif genes.** *J Virol* 1995, **69**:4166-4172.

Gene 432 (2009) 60–66

Contents lists available at ScienceDirect

Gene

journal homepage: www.elsevier.com/locate/gene

# Molecular cloning and characterization of the common marmoset huntingtin gene

Hirohiko Hohjoh [a,*], Hirofumi Akari [b], Yuko Fujiwara [a,c], Yoshiko Tamura [a], Hirohisa Hirai [d], Keiji Wada [c]

[a] Department of Molecular Genetics, National Institute of Neuroscience, NCNP, 4-1-1 Ogawahigashi, Kodaira, Tokyo 187-8502, Japan
[b] Laboratory of Disease Control, Tsukuba Primate Research Center, National Institute of Biomedical Innovation, Tsukuba, Ibaraki, Japan
[c] Department of Degenerative Neurological Diseases, National Institute of Neuroscience, NCNP, Kodaira, Tokyo, Japan
[d] Primate Research Institute, Kyoto University, Inuyama, Aichi, Japan

ARTICLE INFO

*Article history:*
Received 24 July 2008
Received in revised form 4 November 2008
Accepted 5 November 2008
Available online 24 November 2008

Received by M. Di Giulio

*Keywords:*
Common marmoset
Huntingtin
Gene silencing
Immortalized cell line

ABSTRACT

We report here for the first time the isolation and identification of the common marmoset (*Callithrix jacchus*) *huntingtin* (*Htt*) gene, whose ortholog in humans is known to be related to Huntington's disease (HD). A 9396 nucleotide complementary DNA (cDNA) carrying the putative full-length open reading frame of the marmoset *Htt* gene was identified, and highly conserved nucleotide and amino acid sequences among primates were observed. Based on this data and using tools evaluated for the detection of the marmoset *Htt* gene, we have demonstrated gene silencing against the expression of endogenous *Htt* gene in immortalized common marmoset mononuclear cells by means of RNA interference (RNAi). Taken together, the data presented here may assist us in realizing a non-human primate HD model with the common marmoset.



## 1. Introduction

Huntington's disease (HD) is an autosomal dominant neurodegenerative disease characterized by progressive and selective neural cell death associated with choreic movement and dementia (Walker, 2007). The responsible gene for HD, the huntingtin (Htt) gene, has been identified on chromosome 4q16.3 (Gusella et al., 1983; Gilliam et al., 1987), and an aberrant length of a CAG triplet repeat in exon 1, followed by expanded tracts of polyglutamine in the Htt polypeptide, is greatly involved in the onset of HD (Huntington's-Disease, 1993). Although the molecular mechanisms of either normal or aberrant Htt protein are still poorly understood, HD model animals (Mangiarini et al., 1996; Kazemi-Esfarjani and Benzer, 2000; von Horsten et al., 2003) and cells (Lunkes and Mandel, 1998) for understanding the pathogenesis of HD and developing therapies have been established by means of genetic engineering based on the genetic information of *Htt*. The use of an animal model that is closely related to humans may be particularly promising.

The common marmoset (*Callithrix jacchus*) is classified into the Callitrichidae family of Platyrrini (New World monkeys) and has been used as a non-human primate experimental animal in various research fields including gene therapy, autoimmune disease, organ transplantation, and pharmacology (Kendall et al., 1998; Doods et al., 2000; Deisboeck et al., 2003; t'Hart et al., 2003). Accordingly, it is worth promoting studies with the common marmoset aimed at overcoming neurodegenerative diseases such as HD, as the animal's close relationship to humans makes it well suited to this kind of study. Indeed, a recent study has generated a non-human primate HD model with the rhesus monkey (*Macaca mulatta*) (Palfi et al., 2007; Yang et al., 2008).

In this report, we describe for the first time the isolation and characterization of a cDNA encoding the putative full-length open reading frame of the common marmoset *Htt* gene, and present experimental data based on the isolated cDNA. The data presented here may provide us with useful information for establishing non-human primate HD models with the common marmoset.

## 2. Materials and methods

### 2.1. Preparation of total RNA

Common marmoset total RNA was isolated from the brain tissue of a stillborn marmoset fetus and immortalized monocytes (described below) using Trizol (Invitrogen). The experiments with the common marmoset complied with protocols approved by the ethical committee for primate research of the National Center of Neurology and Psychiatry and adhered to the legal requirements of Japan.

*Abbreviations:* HD, Huntington's disease; Htt, huntingtn; RNAi, RNA interference; cDNA, complementary DNA; PBMC, peripheral blood mononuclear cell; RT, reverse transcription; PCR, polymerase chain reaction; ORF, open reading frame; APP, amyloid precursor protein; GAPDH, glyceraldehyde-3-phosphate dehydrogenase; GFP, green fluorescence protein; CMV, Cytomegalovirus.

* Corresponding author.
*E-mail address:* hohjohh@ncnp.go.jp (H. Hohjoh).

0378-1119/$ – see front matter © 2008 Elsevier B.V. All rights reserved.
doi:10.1016/j.gene.2008.11.012

### 2.2. Established common marmoset cell lines

Adult common marmosets being reared at the Primate Research Institute of Kyoto University or Tsukuba Primate Research Center were anesthetized by ketamine, which was approved by the Animal Welfare and Animal Care Committees of both institutes, and peripheral blood was collected. From the collected blood samples, peripheral blood mononuclear cells (PBMCs) were purified and immortalized by infection of a 488-77 strain of *Herpesvirus saimiri* (kindly provided by Dr. R. C. Desrosiers) as previously described (Akari et al., 1996). The established marmoset cell lines, designated HSCj-110, HSCj-009, and HSCj-002, were phenotypically activated CD3+T lymphocytic cells and grown in RPMI-1640 medium (Sigma) supplemented with 10% FCS, 50 mM 2-mercaptoethanol, and antibiotics.

### 2.3. Reverse transcription – (real time) polymerase chain reaction [RT-(real time) PCR]

The common marmoset total RNAs were subjected to complementary DNA (cDNA) synthesis using oligo(dT) primers and a Superscript III reverse transcriptase (Invitrogen), according to the manufacturer's instructions, and polymerase chain reaction (PCR) using the cDNAs as templates was carried out by means of the ABI GeneAmp PCR system 9700 (Applied Biosystems). In the case of real time PCR, the cDNAs were examined by the AB 7300 Real Time PCR System (Applied Biosystems) with a TaqMan Universal PCR Master Mix together with Assays-on-Demand Gene Expression products (Applied Biosystems) or a SYBR Green PCR Master Mix together with Perfect Real Time Primers (Takara Bio) or designed PCR primers, according to the manufacturers' instructions. Synthesized oligonucleotide primers and purchased primer and probe were as follows:

Synthesized oligonucleotide primers:

HD1-F: 5′-TATAGAATTCGGGAGACCGCCATGGCGAC-3′
HD1-ORF-R: 5′-TCAAGCGGCCGCTCAGCAGGTGGTGACCTTG-3′
HD1-1900R2: 5′-TAAAGGATCCCCGTCTAACACAATTTCAG-3′
cjHtt(1139)-F: 5′-TTATAGCTGGAGGCGGTTCC-3′
cjHtt(1254)-R: 5′-GACGTCCGACCTCGATTCAG-3′

Purchased primer and probe:

Assays-on-Demand Gene Expression product for the human *Htt* gene (Assay ID: Hs00169273_m1) (Applied Biosystems).

Perfect Real Time Primers for the human *GAPDH* gene (Primer-Set ID: HA067812) (Takara Bio).

### 2.4. Cloning and sequence analysis of the full-length ORF of the marmoset Htt gene

Complementary DNA derived from the common marmoset total RNA was subjected to PCR amplification using *TaKaRa LA Taq* polymerase (TAKARA BIO) with the HD1-F and HD1-ORF-R primers under the following thermal cycling conditions: heat denaturation at 94 °C for 1 min, 30 cycles of amplification including denaturation at 94 °C for 20 s and extension at 68 °C for 12 min, and a final extension at 72 °C for 10 min. The PCR product was examined by agarose gel electrophoresis followed by ethidium bromide staining, and an approximately 9.4 kb PCR band (Fig. 1) was purified from the gels using a TOPO XL gel purification kit (Invitrogen). The resultant PCR product was inserted into the pCR-XL-TOPO plasmid with a TOPO XL PCR cloning kit (Invitrogen) and then sequence determination of the insert was carried out. To clarify uncertain nucleotide sequences, additional RT-PCR targeting of uncertain regions followed by sequence determination was performed and the precise nucleotide sequence was confirmed. The determined nucleotide sequence encoding a putative full-length ORF of the common marmoset *Htt* gene has been registered in the GenBank database: accession number, AB443866.

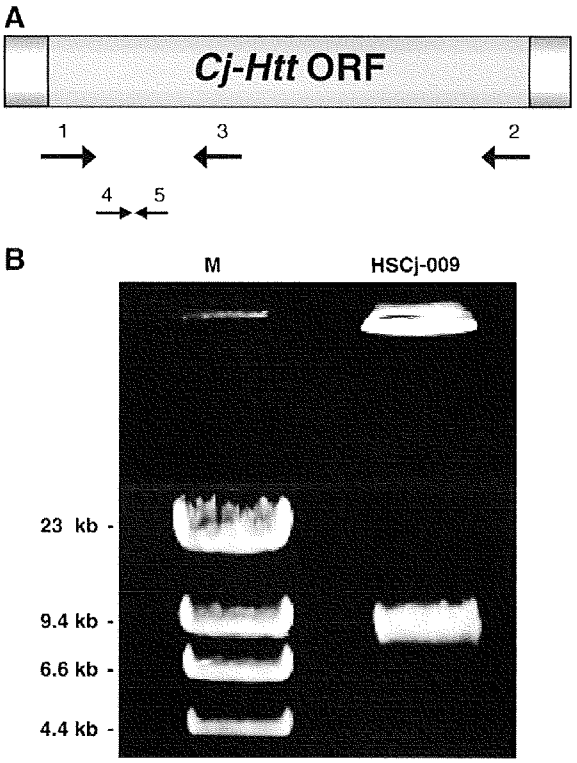


**Fig. 1.** RT-PCR amplification. (A) Schematic drawing of putative *Htt* cDNA. Open reading frame (ORF) is indicated by a yellow box. Arrows indicate synthesized PCR primers, which are designed in possibly conserved nucleotide sequences: 1, HD1-F; 2, HD1-ORF-R; 3, HD1-1900R2; 4, cjHtt(1139)-F; 5, cjHtt(1254)-R (detailed in Materials and methods). (B) RT-PCR. The first strand cDNA was synthesized by RT using RNA isolated from immortalized common marmoset mononuclear cells (HSCj-009) as a template and oligo(dT) as a primer. The following PCR was carried out using HD1-F and HD1-ORF-R primers. The resultant PCR products were analyzed by gel electrophoresis with 0.6 % agarose gel followed by ethidium bromide staining. Hind III-digested λDNA was used as a DNA size marker (M).

### 2.5. Western blotting

Equal amounts (~35 μg) of protein extracts from the common marmoset and mouse brain tissues and established PBMC lines (described above) were separated by SDS-PAGE with 5% polyacrylamide gels and electrophoretically blotted onto PVDF membranes (Millipore). Membranes were blocked for 1 h in blocking solution [5% non-fat milk in TBST buffer (25 mM Tris-HCl, pH 7.4, 150 mM NaCl and 0.1% Tween-20)] and incubated with 1/1000 dilution of mouse anti-huntingtin protein monoclonal antibodies [MAB2166 and MAB2170 (Chemicon); ab7666 (Abcam)] followed by washing in TBST buffer and further incubation with sheep anti-mouse Ig, HRP-linked whole Ab (GE Healthcare). Antigen-antibody complexes were visualized using ECL plus Western Blotting Detection Reagent (GE Healthcare). After detection of signals, the membranes were subjected to antibody removal in Re-Blot Plus strong antibody stripping solution (Chemicon) followed by washing in TBST buffer, and then incubated with 1/1000 dilution of mouse anti-APP [MAB348 (Chemicon)] monoclonal antibody. Subsequent processes were the same as described above.

### 2.6. Gene silencing of marmoset Htt by RNA interference

To monitor gene silencing against the common marmoset *Htt* gene, we constructed a reporter plasmid carrying the 5′-terminal region of the marmoset *Htt* linked with the *GFP* reporter gene: the PCR product obtained from RT-PCR with the HD1-F and HD1-1900R2 primers was

**Table 1**
Sequence homologies (%) among various species' *Htt* genes

| *Homo sapiens* | *Callithrix jacchus* | *Canis lupus familiaris* | *Bos taurus* | *Sus scrofa* | *Mus musculus* | *Rattus norvegicus* |
|---|---|---|---|---|---|---|
| *Homo sapiens* | **95.1**<br>**97.0** | 87.0<br>92.0 | 84.0<br>89.5 | 84.1<br>88.6 | 86.1<br>91.2 | 85.8<br>91.2 |
| *Canis lupus familiaris* | | 86.6<br>91.4 | 84.0<br>88.4 | 83.9<br>87.9 | 85.6<br>90.8 | 85.1<br>90.9 |
| *Callithrix jacchus* | | | 84.5<br>89.4 | 84.4<br>89.7 | 84.0<br>89.2 | 83.8<br>89.3 |
| *Bos taurus* | | | | 86.8<br>89.3 | 81.2<br>87.1 | 81.3<br>87.4 |
| *Sus scrofa* | | | | | 80.9<br>86.9 | 80.8<br>87.2 |
| *Mus musculus* | | | | | | 95.9<br>97.6 |
| *Rattus norvegicus* | | | | | | |

Figures in upper and lower stands represent nucleotide and amino acid sequence homologies, respectively, between two species.

trimmed with EcoRI and BamHI, and inserted into the pd2EGFP-N1 plasmid (Clontech) treated with the same restriction enzymes. The resultant reporter (5′*Cj-Htt-GFP*) plasmid and synthetic siRNA duplex targeting the marmoset *Htt* (cjHtt-1 siRNA duplex) were cotransfected into mouse neuroblastoma Neuro2a cells by Lipofectamine 2000 transfection reagent (Invitrogen) as described previously (Sakai and Hohjoh, 2006). Two days after transfection, the cells were examined by a fluorescent microscope. When the endogenous marmoset *Htt* gene was inhibited by RNAi, the cjHtt-1 siRNA duplex (0.4 nmol/transfection) was introduced into HSCj-009 cells ($1 \times 10^6$ cells/transfection) by means of a Nucleofector system (Amaxa Biosystems) according to the manufacturer's instructions. Two days after transfection, total RNA and cell lysate were prepared from the cells and examined by RT-real time PCR and Western blotting, respectively.

The nucleotide sequences of synthesized cjHtt-1 siRNA were as follows:

Sense: 5′-GCCUUUGAGUCCCUCAAGUUU-3′
Antisense: 5′-ACUUGAGGGACUCAAAGGCUU-3′

### 2.7. Sequence data and computational analyses

The *Htt* sequnece data derived from various species were as follows [GenBank accession number]: human (*Homo sapiens*) [NM_002111]; chimp (*Pan troglodytes*) [XM_517080]; rhesus macaque (*Macaca mulatta*) [XM_001086119]; canine (*Canis lupus familiaris*) [XM_536221]; bovine (*Bos taurus*) [XM_866758]; wild boar (*Sus scrofa*) [NM_213964]; mouse (*Mus musculus*) [NM_010414]; rat (*Rattus norvegicus*) [XM_573634]; chicken (*Gallus gallus*) [XM_420822]. Although the rhesus macaque Htt sequence [XM_001086119] contains 20 undetermined nuclotides at positons 4932–4951 followed by 6 suspensive amino acid sequences, the sequence was used and examined together with the other sequneces in this study.

Sequence homology analysis of either nucleotide or amino acid sequences was carried out by means of the GENETYX software (Software Development Co., Ltd., Tokyo, Japan), where all the parameters were set at default. For identification of the HEAT repeats in the Cj-Htt protein sequences, the REP program (http://www.embl-heidelberg.de/~andrade/papers/rep/search.html) developed by Andrade et al. was used.

## 3. Results and discussion

### 3.1. Isolation and characterization of the common marmoset Htt gene

To isolate and identify the common marmoset *Htt* (*Cj-Htt*) gene and/or gene products, we focused on conserved regions in the *Htt* gene and isolate cDNA clone of the *Cj-Htt* transcript. Highly homologous regions (sequences) between the human and mouse *Htt* genes, whose corresponding regions in the *Cj-Htt* gene were also expected to remain conserved, were selected, and PCR primers were designed for such regions. We add that such conserved regions are also detectable by BLAST search with the human *Htt* as a query on the Trace archive of the Cj-database in NCBI. RT-PCR with the designed primers and total RNA extracted from common marmoset brain tissue and established cell lines was carried out, and an approximately 9.4 kb long PCR product, which was expected to contain the full-length open reading frame (ORF) of *Cj-Htt*, was obtained (Fig. 1). The PCR product was subjected to sequence determination and then compared with various species' *Htt* genes. From the results, it was clear that the PCR product, which is 9396 nucleotides in length, was derived from the common marmoset *Htt* gene which encodes a predicted 3131 amino acid long Cj-Htt polypeptide (the sequence accession number in GenBank is AB443866). Sequence homologies in the *Htt* gene among various species are indicated in Table 1. From the data, it appears that both the nucleotide and predicted amino acid sequences of the *Cj-Htt*

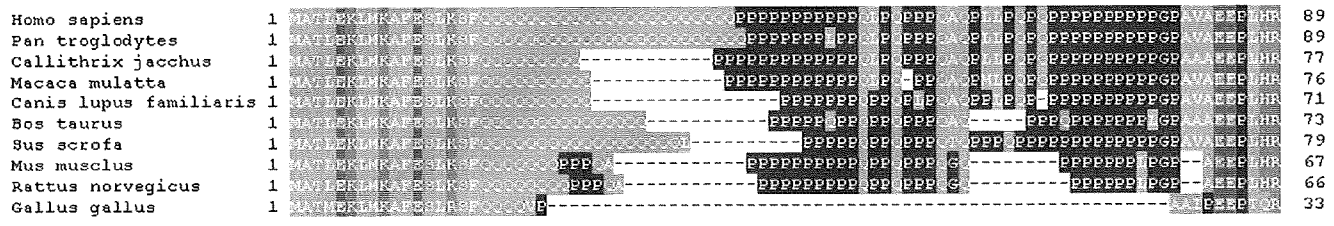


**Fig. 2.** Alignment of amino acid sequences in the Htt exon 1 and its corresponding regions. Sequence data were aligned based on the human Htt exon 1 (top line). Amino acid residues are color-coded based on the biochemical properties of the residues: hydrophobic amino acids in orange, polar amino acids with uncharged R groups in green, acidic amino acids in pink, basic amino acids in light blue, and special amino acids in dark blue.

**Table 2**
Alignment of HEAT repeats

| Repeat* | Species** | AA position | | Fragment † | Score | E-value |
|---|---|---|---|---|---|---|
| | | From | To | | | |
| HEAT_AAA | Hs - Htt | 124 | 162 | QKLLGIAMELFLLCSDDAESDVRMVADECLNKVIKALMD | 1510 | 1.26E-06 |
| | Cj - Htt | 112 | 150 | QKLLGIAMELLLLCSDDAESDVRMVADECLNKVIKALMD | 1590 | 5.48E-07 |
| HEAT_AAA | Hs - Htt | 205 | 243 | RPYLVNLLPCLTRTSKRPEESVQETLAAAVPKIMASFGN | 1990 | 1.03E-04 |
| | Cj - Htt | 193 | 231 | RPYLVNLLPCLTRTSKRPEESVQETLAAAVPKIMASFGN | 1990 | 2.37E-08 |
| HEAT_AAA | Hs - Htt | 247 | 285 | DNEIKVLLKAFIANLKSSSPTIRRTAAGSAVSICQHSRR | 1590 | 5.48E-07 |
| | Cj - Htt | 235 | 273 | DNEIKILLKAFIANLKSSSPTIRRTAAGSAVSICQHSRR | 1590 | 1.97E-06 |
| HEAT_AAA | Hs - Htt | 317 | 355 | LLTLRYLVPLLQQQVKDTSLKGSFGVTRKEMEVSPSAEQ | 1620 | 1.11E-06 |
| | Cj - Htt | 305 | 343 | LLTLRYLVPLLHQQVKDTSLKGSFGVTRKEMEVSPSAEQ | 1570 | 1.46E-07 |
| HEAT_ADB | Hs - Htt | | | | | |
| | Cj - Htt | 734 | 771 | YPEEQYVSDILNYIDHGDPQVRGATAILCGTLVCSILS | 1450 | 3.29E-07 |
| HEAT_AAA | Hs - Htt | 803 | 841 | TFSLADCIPLLRKTLKDESSVTCKLACTAVRNCVMSLCS | 1500 | 5.78E-07 |
| | Cj - Htt | 791 | 829 | TFSLADCVPLLRKTLKDESSVTCKLACTAVRHCVMSLCS | 1449 | 2.90E-06 |
| HEAT_AAA | Hs - Htt | 904 | 942 | KLQERVLNNVVIHLLGDEDPRVRHVAAASLIRLVPKLFY | 1930 | 6.69E-08 |
| | Cj - Htt | 892 | 930 | TLQERVLTSVVIHLLGDEDPRVRHVAAASLIRLVPKLFY | 2150 | 2.51E-05 |
| HEAT_AAA | Hs - Htt | 984 | 1025 | RIYRGYNLLPSITDVTMENNLSRVIAAVSHELITSTTRALTF | 1370 | 9.05E-06 |
| | Cj - Htt | 972 | 1013 | RIYRGYNLLPSIIDVTMENNLSRVIAAVSHELITSTTRALTF | 1410 | 2.71E-06 |
| HEAT_AAA | Hs - Htt | 1425 | 1463 | RLFEPLVIKALKQYTTTTCVQLQKQVLDLLAQLVQLRVN | 1370 | 5.62E-06 |
| | Cj - Htt | 1413 | 1451 | RLFEPLVIKALKQYTTTTSVQLQKQVLDLLAQLVQLRVN | 1580 | 3.20E-07 |
| HEAT_AAA | Hs - Htt | 2798 | 2836 | DDTAKQLIPVISDYLLSNLKGIAHCVNIHSQQHVLVMCA | 1430 | 3.51E-06 |
| | Cj - Htt | 2785 | 2823 | DDTAKQLIPVISDYLLSSLKGLAHCVNTHSQQHVLVMCA | 1430 | 3.29E-06 |

* HEAT_AAA and HEAT_ADB indicate subsets of HEAT repeats representing PP2A and adaptin families, respectively.
** Hs-Htt and Cj-Htt indicate the human and common marmoset Htt proteins, respectively.
†Amino acids which are different from the sequence of Hs-Htt are indicated in red.

cDNA have significant sequence homology to that of other species' *Htt* genes. In addition, it should be noted that *Htt* sequences between the human and common marmoset (colored in yellow in Table 1) appear to be particularly conserved as compared with sequence conservation within non-primate *Htt* genes, suggesting that the *Htt* gene is highly conserved in primates.

Fig. 2 shows the alignment of amino acid sequences encoded by *Htt* exon 1 and its corresponding region in various species. From the alignment, *Cj-Htt* appears to possess a short polyglutamine tract of nine glutamines compared with that of the human and chimpanzee *Htt* genes; but other than the polyglutamine tract, the exon 1 corresponding region in *Cj-Htt* exhibits high sequence homology to the human *Htt* exon 1. It is also interesting that polyproline region adjacent to the polyglutamine tract has differences between primates and non-primates: amino acid substitutions and deletions are observed, and the lack of the polyproline region in the *Gallus gallus Htt* exon 1 is particularly remarkable. These differences may influence folding and aggregation of the Htt protein, and might represent adaptive evolution of *Htt* to each species. The difference in the exon 1 among various species may provide us with a hint for understanding the expansion of the polyglutamine tract in Huntington's disease in human.

Other than the exon 1 region, we also investigated the HEAT repeats possessing tandem arrayed bihelical structure, which appear to wrap around target substrates (Andrade and Bork, 1995; Neuwald and Hirano, 2000), and found that the HEAT repeats are also conserved in the Cj-Htt protein (Table 2). In addition, it may be interesting that HEAT_ADB, a subset of HEAT repeats representing adaptin family, is present in Cj-Htt, but not in Hs-Htt.

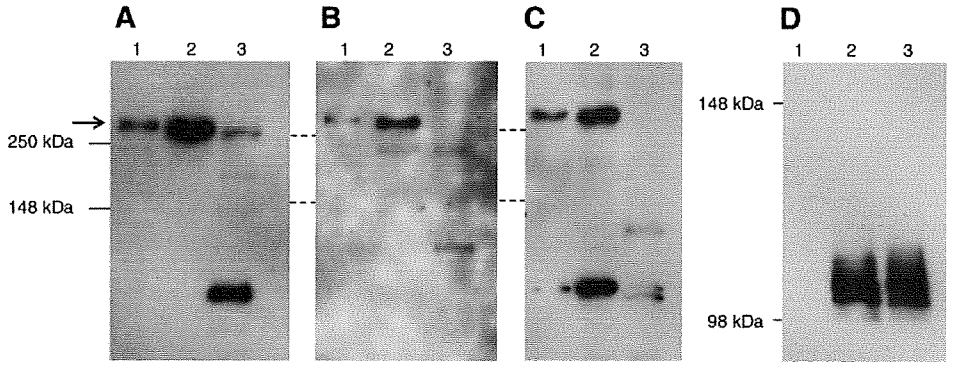


**Fig. 3.** Assessment of anti-human Htt antibodies against the common marmoset Htt polypeptide. Cell lysate derived from the common marmoset cell line (HSCj-110) (lane 1), brain tissue (lane 2), and mouse brain tissue as a control (lane 3) was examined by Western blotting with anti-human Htt antibodies. Tested antibodies were as follows: (A) MAB2166 (Chemicon), (B) MAB2170 (Chemicon), and (C) ab7666 (Abcam). Arrow indicates the signals of Htt proteins. The same results as those of HSCj-110 were also obtained when HSCj-002 and-009 were used (data not shown). After detection of signals, blotted membranes were subjected to antibody removal and then incubated with anti-APP antibody [MAB348 (Chemicon)] (D) followed by the same procedure as in the anti-human Htt antibodies described above.

### 3.2. Detection of Cj-Htt gene products

It is important to be able to properly detect the *Cj-Htt* gene and its gene products. Since the nucleotide and predicted amino acid sequences of the *Cj-Htt* cDNA showed significantly high sequence homologies to those of the human *Htt* gene, we tested whether commercially-available TaqMan probe and antibodies against human *Htt* gene products (mRNA and protein) were also able to detect *Cj-Htt* gene products. As a result, the TaqMan probe (Fig. 5A) appears to be able to detect *Cj-Htt* mRNA. In addition, newly designed PCR primers, which are perfectly matched to *Cj-Htt*, also appear to be able to detect *Cj-Htt* mRNA (Fig. 5B).

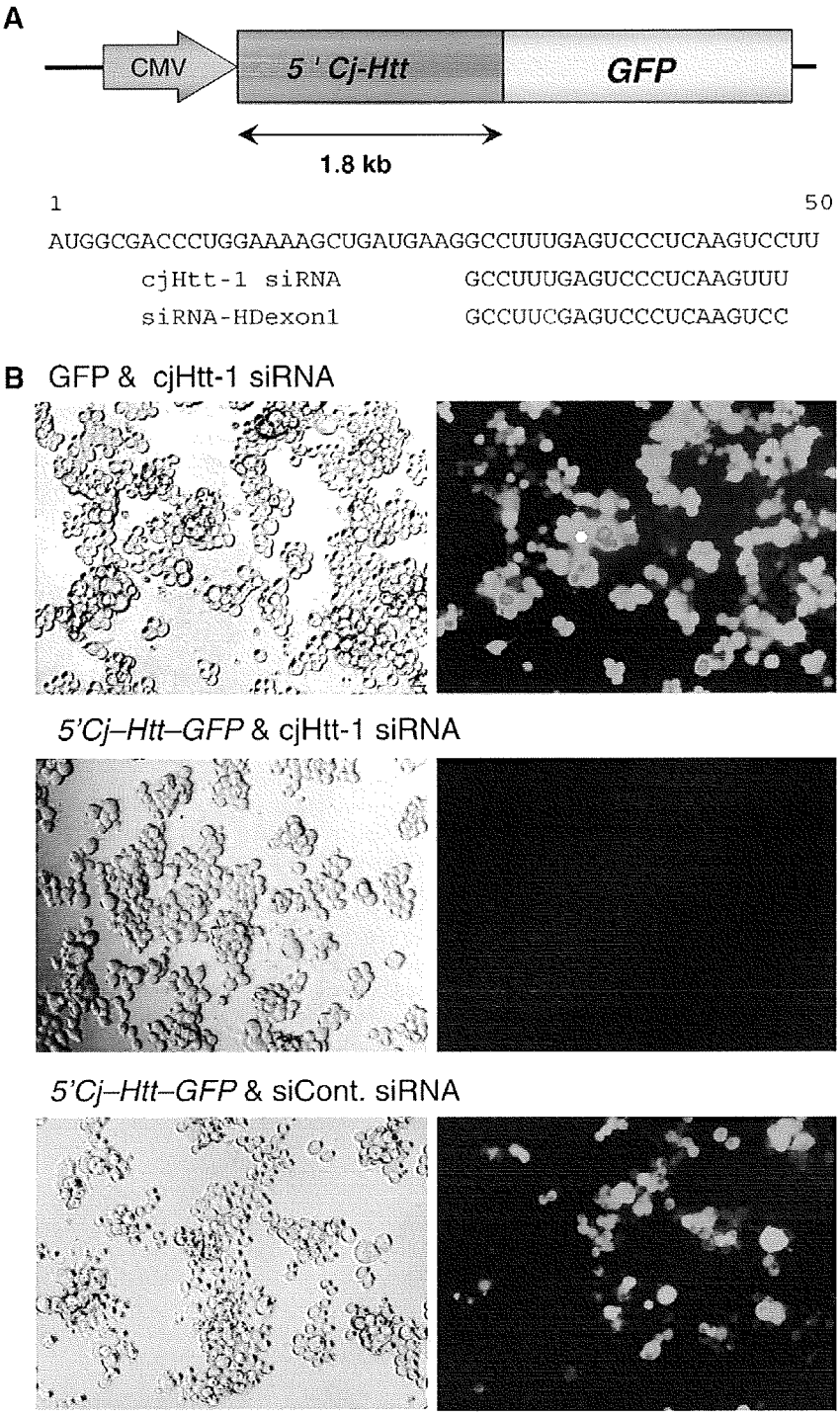


**Fig. 4.** Gene silencing against the 5′*Cj-Htt-GFP* fusion gene. (A) Schematic drawing of the 5′*Cj-Htt-GFP* fusion gene and designed cjHtt-1 siRNA. The fusion gene is composed of the 5′ terminal region of the Cj-Htt ORF and GFP, and driven by the Human cytomegalovirus promoter. The *Cj-Htt* sequence from the first ATG to position 50 is shown together with sequences of cjHtt-1 siRNA and siRNA-HDexon1 targeting human *Htt*. A variant nucleotide between the siRNAs is indicated in red. (B) Effect of cjHtt-1 siRNA on gene silencing. Reporter genes [5′*Cj-Htt-GFP* or *GFP* (empty reporter)] and siRNAs [cjHtt-1 or siCont (non-silencing siRNA)] were introduced into mouse neuroblastoma Neuro2a (N2a) cells. Two days after transfection, the cells were examined by a fluorescent microscope. Left (differential interference contrast) and right (fluorescence image) panels are identical in the visual field.

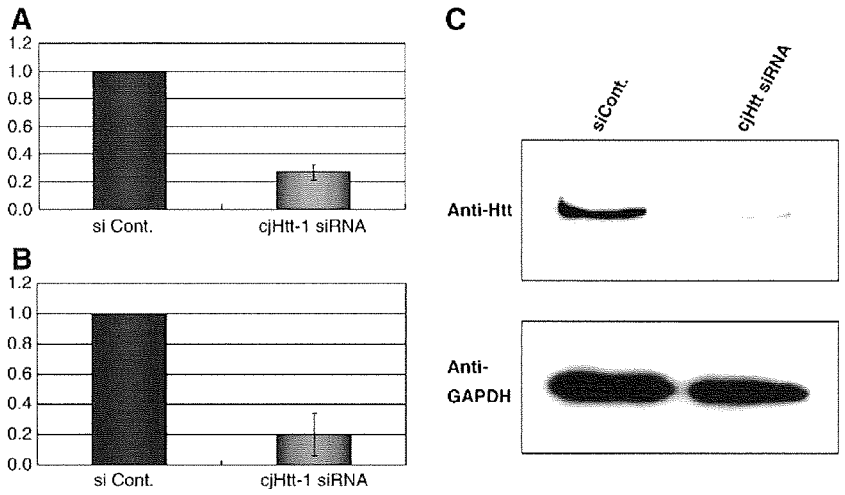


**Fig. 5.** Inhibition of expression of endogenous *Cj-Htt* by RNAi. The cjHtt-1 siRNA was introduced into HSCj-009 cells by means of electroporation. Two days after transfection, total RNA and cell lysate were prepared and examined by RT-real time PCR and Western blotting, respectively. Total RNA was subjected to cDNA synthesis as in Fig. 1. The resultant cDNA was examined by real time PCR with a TaqMan probe for the human *Htt* gene (A) and newly designed PCR primers [cjHtt(1139)-F and cjHtt(1254)-R] (B). The expression of *Gapdh* as a control was also examined using Perfect Real Time Primers for the human *GAPDH* gene (TAKARA BIO). The expression level of *Cj-Htt* was normalized against that of *Gapdh*, and the ratios of *Cj-Htt* expression level in the presence of cjHtt-1 siRNA were normalized against the ratio obtained in the presence of the siControl siRNA (siCont.). Data are means of at least three independent determinations. Error bars represent standard deviations. (C) Western blot. Cell lysate was examined by Western blotting with anti-human Htt antibody (MAB2166; Chemicon) as in Fig. 3. After detection of signals, the expression of GAPDH as a control was also examined by anti-GAPDH antibody (AM4300; Ambion).

Western blot analyses indicate that a polypeptide of approximately 350 kDa, which is almost the same as the molecular weight estimated from the amino acid sequence (346 kDa) in the *Cj-Htt* cDNA, can be detected in the common marmoset specimens by the antibodies tested, suggesting that the Cj-Htt protein is detectable with the antibodies (Figs. 3A–C). The 350 kDa mouse Htt protein was detected by the MAB2166 antibody (Fig. 3A), but hardly with the other antibodies (Figs. 3B and C). This may be caused by possibly low expression level of mouse Htt in the brain tissue, and/or by difference in the epitope sequences between the common marmoset and mouse Htt proteins. Other than the 350 kDa band, a few bands migrated faster than the 350 kDa band were also observed. They may be degradation products of the Htt protein, and different cells and/or species might have different degradation of the protein. To clarify these, further studies need to be carried out.

In addition to the Htt protein, we also examined the expression of amyloid precursor protein (App) with the 22C11 antibody, which can recognize the same amino acid sequence at positions 66–81 of either the human or mouse App. As a result, the App signal was able to be detected in either the common marmoset or mouse brain tissue, but not in the common marmoset immortalized peripheral blood mononuclear cells (PBMCs) (Fig. 3D), suggesting little or no expression of App in PBMCs and availability of the antibody for detection of the Cj-App protein.

### 3.3. Gene silencing against the Cj-Htt gene

To verify the data presented here and tools for the detection of *Cj-Htt*, we carried out gene silencing against the expression of endogenous *Cj-Htt* by means of RNA interference (RNAi), and assessed the knockdown potency of designed siRNA targeting *Cj-Htt* using the tools evaluated above. Based on a previous study where a competent siRNA duplex, siRNA-HDexon 1, conferring strong inhibition against the expression of the human *Htt* gene was used (Liu et al., 2003), we chemically synthesized an siRNA duplex, cjHtt-1 siRNA, corresponding to the siRNA-HDexon 1 duplex; note that there is one nucleotide change between cjHtt-1 siRNA and siRNA-HDexon 1 (Fig. 4A).

To examine the effect of the siRNA duplex on gene silencing, we constructed a reporter plasmid carrying the 5′ terminal region of *Cj-Htt* cDNA linked with the *GFP* reporter gene (the 5′*Cj-Htt-GFP* fusion gene). The reporter plasmid and the siRNA were cotransfected into mouse Neuro2a cells, and the expression of the 5′*Cj-Htt-GFP* fusion gene was examined by a fluorescent microscope. As shown in Fig. 4B, the data indicated that the cjHtt-1 siRNA duplex was able to induce strong RNAi activity against the fusion gene expression.

Next, we introduced the cjHtt-1 siRNA duplex into immortalized common marmoset mononuclear cells by means of electroporation, and two days after transfection, the expression levels of the endogenous *Cj-Htt* mRNA and protein were examined by RT-real time PCR and Western blotting, respectively. As shown in Fig. 5, the results consistently indicated that *Cj-Htt* mRNA (A and B) and protein (C) levels markedly decreased in the presence of the cjHtt-1 siRNA duplex, i.e., potent RNAi knockdown against the endogenous *Cj-Htt* gene was induced by the siRNA duplex. Finally, the data presented here also indicate that proper detection of the newly identified *Cj-Htt* gene and its products can be performed by means of the methods and tools assessed in this study.

In conclusion, we described for the first time the common marmoset *Htt* gene, and also detection methods and tools for the gene and its gene products. The data presented here may assist us in promoting a non-human primate HD model with the common marmoset.

## Acknowledgments

We would like to thank Dr. R.C. Desrosiers for kindly providing HS viruses. We also thank Drs. K. Nakamura, T. Kabuta, M. Suzuki, and C. Konya for their helpful advice and discussion. Finally, we would like to thank Dr I. Kanazawa for his encouragement and helpful advice. This work was supported by research grants from the Ministry of Health, Labour and Welfare of Japan.

## References

Akari, H., et al., 1996. In vitro immortalization of Old World monkey T lymphocytes with Herpesvirus saimiri: its susceptibility to infection with simian immunodeficiency viruses. Virology 218, 382–388.

Andrade, M.A., Bork, P., 1995. HEAT repeats in the Huntington's disease protein. Nat. Genet. 11, 115–116.

Deisboeck, T.S., et al., 2003. Development of a novel non-human primate model for preclinical gene vector safety studies. Determining the effects of intracerebral HSV-1 inoculation in the common marmoset: a comparative study. Gene Ther. 10, 1225–1233.
Doods, H., et al., 2000. Pharmacological profile of BIBN4096BS, the first selective small molecule CGRP antagonist. Br. J. Pharmacol. 129, 420–423.
Gilliam, T.C., et al., 1987. A DNA segment encoding two genes very tightly linked to Huntington's disease. Science 238, 950–952.
Gusella, J.F., et al., 1983. A polymorphic DNA marker genetically linked to Huntington's disease. Nature 306, 234–238.
Huntington's-Disease, C.R.G.o., The Huntington's Disease Collaborative Research Group, 1993. A novel gene containing a trinucleotide repeat that is expanded and unstable on Huntington's disease chromosomes. Cell 72, 971–983.
Kazemi-Esfarjani, P., Benzer, S., 2000. Genetic suppression of polyglutamine toxicity in Drosophila. Science 287, 1837–1840.
Kendall, A.L., Rayment, F.D., Torres, E.M., Baker, H.F., Ridley, R.M., Dunnett, S.B., 1998. Functional integration of striatal allografts in a primate model of Huntington's disease. Nat. Med. 4, 727–729.
Liu, W., Goto, J., Wang, Y., Murata, M., Wada, K., Kanazawa, I., 2003. Specific inhibition of Huntington's disease gene expression by siRNAs in cultured cells. Proc. Jpn. Acad. 79, 293–298.
Lunkes, A., Mandel, J.L., 1998. A cellular model that recapitulates major pathogenic steps of Huntington's disease. Hum. Mol. Genet. 7, 1355–1361.
Mangiarini, L., et al., 1996. Exon 1 of the HD gene with an expanded CAG repeat is sufficient to cause a progressive neurological phenotype in transgenic mice. Cell 87, 493–506.
Neuwald, A.F., Hirano, T., 2000. HEAT repeats associated with condensins, cohesins, and other complexes involved in chromosome-related functions. Genome Res. 10, 1445–1452.
Palfi, S., et al., 2007. Expression of mutated huntingtin fragment in the putamen is sufficient to produce abnormal movement in non-human primates. Mol. Ther. 15, 1444–1451.
Sakai, T., Hohjoh, H., 2006. Gene silencing analyses against amyloid precursor protein (APP) gene family by RNA interference. Cell Biol. Int. 30, 952–956.
t'Hart, B.A., Vervoordeldonk, M., Heeney, J.L., Tak, P.P., 2003. Gene therapy in nonhuman primate models of human autoimmune disease. Gene Ther. 10, 890–901.
von Horsten, S., et al., 2003. Transgenic rat model of Huntington's disease. Hum. Mol. Genet. 12, 617–624.
Walker, F.O., 2007. Huntington's disease. Lancet 369, 218–228.
Yang, S.H., et al., 2008. Towards a transgenic model of Huntington's disease in a non-human primate. Nature 453, 921–924.

# Efficient inhibition of SDF-1α-mediated chemotaxis and HIV-1 infection by novel CXCR4 antagonists

Yuki Iwasaki,[1] Hirofumi Akari,[1,4] Tsutomu Murakami,[2] Sei Kumakura,[3] Md. Zahidunnabi Dewan,[2,5] Mikiro Yanaka[3,6] and Naoki Yamamoto[2]

[1]Laboratory of Disease Control, Tsukuba Primate Research Center, National Institute of Biomedical Innovation, Tsukuba; [2]AIDS Research Center, National Institute of Infectious Diseases, Tokyo; [3]Biomedical Research Laboratories, Kureha Corporation, Tokyo, Japan

(Received November 11, 2008/Revised December 25, 2008/Accepted December 25, 2008/Online publication February 24, 2009)

**CXC chemokine receptor-4, the receptor for stromal cell-derived factor-1α as well as human immunodeficiency virus type 1, belongs to the chemokine receptor family and has been shown to play a critical role in directing the migration of cancer cells to sites of metastasis as well as human immunodeficiency virus type 1 infection. We had previously reported that a duodenally absorbable CXC chemokine receptor-4 antagonist, KRH-1636, showed a potent anti-human immunodeficiency virus type 1 activity both *in vivo* and *in vitro*. In this study, we initially examined the effect of the compound and its derivatives on stromal cell-derived factor-1α-mediated chemotaxis of cancer cells in order to evaluate if they could be applicable as a novel inhibitor of cancer metastasis. We found that both KRH-2731 and KRH-3955 were highly potent antagonists of stromal cell-derived factor-1α-mediated chemotaxis, i.e. the derivatives exhibited 50% effective concentrations of less than 10 nM, for more than 1000-fold efficacy improvement over the prototype KRH-1636. We further demonstrated the greater anti-human immunodeficiency virus type 1 efficacy of the derivatives compared with the original KRH-1636. Taken together, the KRH-1636 derivatives KRH-2731 and KRH-3955 may be promising as a novel inhibitory drug for cancer metastasis as well as for human immunodeficiency virus type 1 infection. (*Cancer Sci* 2009; 100: 778–781)**

Chemokines are secretory proteins with a molecular weight of about 8–14 kDa, and are generally alkaline and heparin-bound. The small chemokine proteins are classified into four highly conserved groups, i.e. CXC, CC, C, and CX3C (X indicates the number of amino acids between the cysteine residues) on the basis of the position of the first two cysteines that are adjacent to the amino terminus.[1] An established role for several members of the CXC and CC chemokine families is to provide directional cues for the movement of leukocytes in development, homeostasis, and inflammation.[2] At the time of the movement of leukocytes, chemokine concentration gradually increases at the inflammatory site because the chemoattractants released from the luminal surface of the endothelium, the inflammatory site of the lymphocyte, are rapidly diluted and swept downstream by blood flow. Leukocytes in the mainstream of blood flow may make contact with the endothelium via a group of molecules called selectins,[3] and may then roll along the endothelial surface.

The cell surface molecule CXC chemokine receptor-4 (CXCR4) is a 7-transmembrane-spanning, G-protein-coupled receptor for the CXC chemokine stromal cell-derived factor-1α (SDF-1α)/pre-B-cell growth stimulating factor (PBSF)/CXCL12.[2] The open reading frame of the *CXCR4* gene encodes a peptide of 352 amino acids and is interrupted by one intron in the region encoding the N-terminal segment.[4]

CXCR4 is a receptor for the SDF-1α. SDF-1α interacts with CXCR4 to play a variety of physiological roles: B-cell formation in liver and bone marrow at the fetal stage, homing of bone marrow cells in the developmental process, formation of the interventricular septum, regulation of movement of the cerebellum granule cell in neurogenesis, and large vasculogenesis that nourishes the gastrointestinal tract.[2] Since both CXCR4 and SDF-1α knockout mice do not survive, the interaction between these molecules is essential in the developmental process.[5–7] It has been reported recently that CXCR7 binds with high affinity to SDF-1α and to interferon-inducible T-cell α-chemoattractant (I-TAC, also known as CXCL11).[8] However, unlike other chemokine receptors, ligand activation of CXCR7 induces neither $Ca^{2+}$ mobilization nor cell migration.[8]

CXCR4 is also shown to be one of the coreceptors for human immunodeficiency virus type 1 (HIV-1).[9] Entry of HIV-1 into target cells involves interactions of the viral envelope protein (Env) with CD4 and a coreceptor, mainly either CXCR4 for T-cell–tropic HIV-1,[10,11] or CCR5 for macrophage–tropic HIV-1.[12,13] In acute HIV-1 infection, primarily macrophage-tropic strains are involved in transmission of the virus, whereas T-cell–tropic strains emerge later and are associated with the rapid progression to AIDS.[9]

Importantly, cancer cells originating from the pancreas, brain, breast, prostate, kidney, ovaries, thyroid, and malignant melanoma express CXCR4; however, normal tissues scarcely express CXCR4. Increasing CXCR4 promotes metastasis of these tumor cells toward SDF-1α-expressing organs including the lungs, liver, lymph nodes, bone marrow, and adrenal glands.[14–17] Further, interaction between CXCR4 and SDF-1α promotes progression of chronic and acute lymphocytic leukemia,[3] and exacerbation of chronic rheumatoid arthritis.[18]

We previously reported that a duodenally absorbable CXCR4 antagonist, KRH-1636, competitively blocked the association of the Env protein of HIV-1 with CXCR4 both *in vivo* and *in vitro* as well as the interaction of SDF-1α with CXCR4.[19] We therefore hypothesized that KRH-1636 could be a promising chemical for offering protection from both cancer metastases induced by SDF-1α and from CXCR4-tropic HIV-1 infection. In order to assess this possibility, we sought to evaluate whether the CXCR4 antagonist KRH-1636 and its derivatives could potently inhibit SDF-1α-mediated chemotaxis of cancer cells as well as HIV-1 infection.

## Materials and Methods

**Reagents.** SDF-1α (R&D systems, Minneapolis, MN, USA) was dissolved in phosphate-buffered saline (PBS) at 1 μM. KRH-1636,[19] and its derivatives KRH-2731, -3148, and -3955 were synthesized at Kureha Chemical Industry (Tokyo, Japan). These

[4]To whom correspondence should be addressed. E-mail: akari@nibio.go.jp
[5]Current address: Department of Pathology, New York University School of Medicine, 550 First Avenue, New York, NY 10016, USA
[6]Current address: Kureha Special Laboratory Co. Ltd. Fukushima 974-8232, Japan
Abbreviations: CXCR4, CXC chemokine receptor-4; DMSO, dimetyl sulfoxide; $EC_{50}$, 50% effective concentration; Env, envelope protein; FACS, fluorescence-activated cell sorter; FCS, fetal calf serum; HIV-1, human immunodeficiency virus type 1; mAb, monoclonal antibody; OD, optical density; PBS, phosphate-buffered saline; PBSF, pre-B-cell growth stimulating factor; PE, phycoerythrin; SDF-1α, stromal cell derived factor-1α.



doi: 10.1111/j.1349-7006.2009.01104.x

compounds were dissolved in dimethyl sulfoxide (DMSO) at a final concentration of 0.1%.

**Cell culture.** Jurkat and its subline Jurkat E6-1 were used in this study. The cells were cultured in a complete medium (CM) composed of RPMI-1640 (Sigma, Tokyo, Japan) supplemented with 10% fetal calf serum (FCS), 100 U/mL penicillin, 100 μg/mL streptomycin, and 0.1% 2-Mercaptoethanol at 37°C in a humidified environment with a 5% $CO_2$ atmosphere.

**Fluorescence-activated cell sorter (FACS) analysis.** Expression of CXCR4 and CD4 on Jurkat cells was measured by flow cytometry. The cells were suspended at $1 \times 10^5$ cells/mL in PBS containing 1% FCS. The cells were reacted with phycoerythrin (PE)-labeled mouse monoclonal antibodies (mAbs) to human CXCR4 (12G5; eBioscience, San Diego, USA) and CD4 (Leu3a; Becton Dickinson, Tokyo, Japan) as a positive control at 4°C for 1 h. The treated cells were washed and fixed with 1% formalin in PBS. Fluorescence of the stained cells was detected by a FACSCalibur (Becton Dickinson), followed by the analysis of fluorescence intensity by CellQuest software (Becton Dickinson).

**Cytotoxic assay.** Jurkat cells were treated with CXCR4 antagonists at 37°C for 1 h. The cells were harvested and resuspended in a 96-well plate. The viability of the treated cells was measured using a Cell Counting Kit-8 (Dojindo, Tokyo, Japan).

**Chemotaxis assay.** Cellular chemotaxis was investigated using a 24-well culture plate with 8-μm-pore filters (Transwell; Corning, Tokyo, Japan). Jurkat cells were washed three times in a FCS-free medium and suspended at $3 \times 10^6$ cells/mL in RPMI-1640 containing 0.1% bovine serum albumin (control medium). The control medium (0.2 mL) containing $3 \times 10^5$ cells was added to the upper well; the control medium (0.6 mL) with or without SDF-1α (100 ng/mL) or CXCR4 antagonists (10 μM) was added to the lower well. The culture plate was incubated for 3 h at 37°C; thereafter, the cells in the upper or lower well were then harvested and resuspended in a 96-well plate. The number of cells in each well was measured using a Cell Counting Kit-8. Optical density (OD) (455 nm/650 nm) values were measured on a microplate reader. The chemotaxis index was calculated as follows: [(OD of treated cells in the lower well – OD of control medium in the lower well)/(OD in sum of the lower and upper wells – OD of control medium in the lower well)] × 100.

For evaluating the inhibitory effect of the CXCR4 antagonists on chemotaxis, cells were pretreated with CXCR4 antagonists at 37°C for 1 h, followed by the chemotaxis assay as stated above.

**Anti-HIV-1 assay.** Human peripheral blood mononuclear cells, which were activated with immobilized anti-CD3 mouse mAb in RPMI-1640 medium supplemented with 10% FCS for 3 days, were infected with NL4-3 at a multiplicity of infection of 0.001. After 3 h of adsorption, the cells were washed, and cultured in CM supplemented with recombinant human interleukin-2 (50 U/mL), in the presence or absence of the test compounds. Amounts of HIV-1 capsid (p24) antigen produced in the culture supernatants were measured by an enzyme-linked immunosorbent assay kit (ZeptoMetrix Corp., Buffalo, NY, USA) 7–10 days after infection.

## Results

The initial purpose of this study was to evaluate whether a series of CXCR4 antagonists could inhibit cancer metastasis, which is promoted by the interaction between SDF-1α and CXCR4. In order to evaluate the antagonistic effect of the compounds, we sought to develop an assay system for quantitatively detecting SDF-1α-mediated chemotaxis induced by the interaction. In this experiment, we employed $CD4^+$ leukemic cell line Jurkat as a $CXCR4^+$ indicator.[20] Since Jurkat sublines have different characteristics, we compared CXCR4 expression in the original Jurkat cells and its subline E6-1 by using flow cytometry. As expected, CXCR4 expression was comparable in both cell lines, while CD4 expression was greater in the Jurkat cells (Fig. 1a).

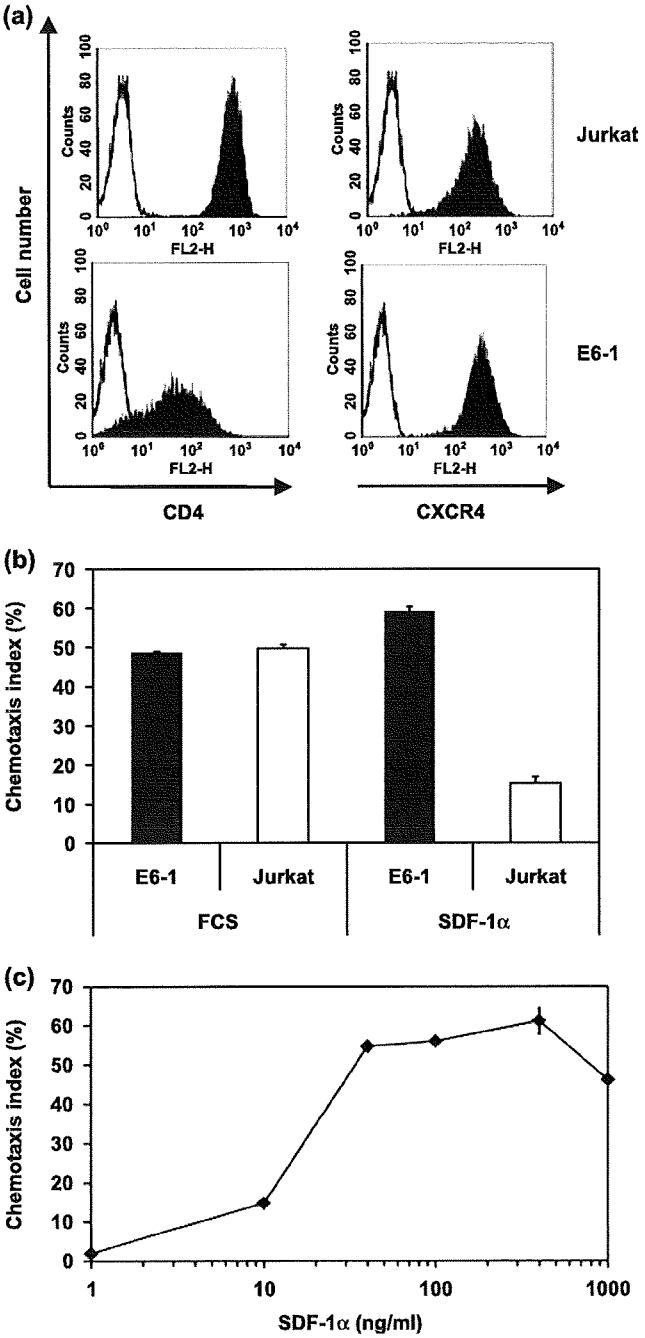


Fig. 1. A quantitative assay system for stromal cell-derived factor-1α (SDF-1α)-mediated chemotaxis. (a) Evaluation of CD4 and CXC chemokine receptor-4 (CXCR4) expression on Jurkat and its subline E6-1. The cells were stained with phycoerythrin-labeled anti-CXCR4 or anti-CD4 mouse monoclonal antibodies. Open and closed lines indicate fluorescence of the control and stained cells, respectively. (b) Effect of SDF-1α on chemotaxis of Jurkat and its subline E6-1. The cell lines were incubated with the control medium including 400 ng/mL of SDF-1α or 10% fetal calf serum (FCS) for 24 h at 37°C. The results are shown as a chemotaxis index and standard deviation. The calculation of the chemotaxis index is described in 'Materials and Methods'. (c) Dose-dependent effect of SDF-1α on the chemotaxis of E6-1 cells. Increasing amounts of SDF-1α were treated with E6-1 cells for 3 h and the levels of migration to the lower well are indicated as a chemotaxis index.

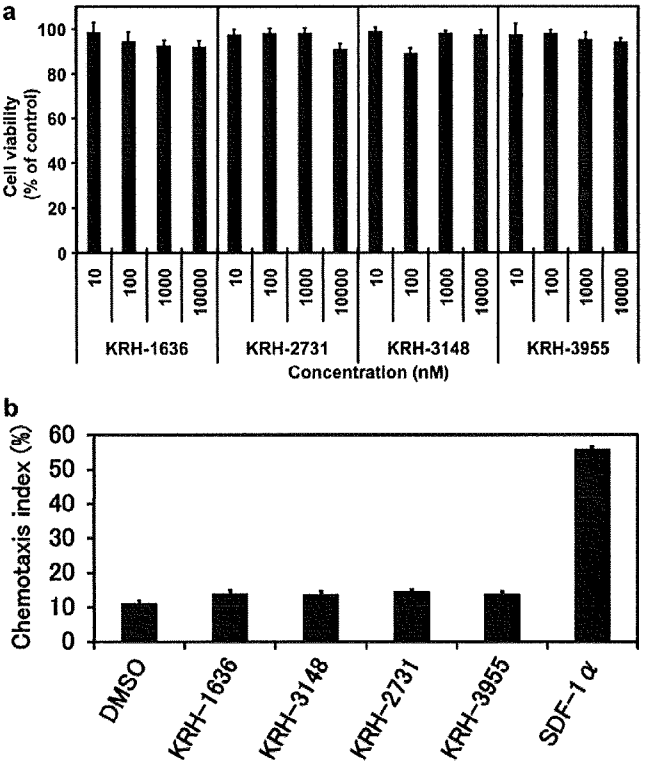


Fig. 2. CXC chemokine receptor-4 (CXCR4) antagonists exhibited neither cytotoxic nor agonistic effects. (a) Increasing amounts of CXCR4 antagonists were examined for their cytotoxic effect on E6-1 cells. (b) CXCR4 antagonists (10 μM) or stromal cell-derived factor-1α (SDF-1α) (100 ng/mL) were added to the lower wells in a chemotaxis assay and were incubated at 37°C for 3 h. The treated E6-1 cells were evaluated for the chemotaxis index. DMSO, dimethyl sulfoxide.

Next, the two cell lines were analyzed for SDF-1α-mediated chemotaxis activity; after 24 h of incubation, about 30% of both Jurkat and E6-1 migrated to the lower wells in the presence of the control medium. Since the value was the background for this chemotaxis assay, we subtracted this value from the subsequent experiments. We decided to use 400 ng/mL of SDF-1α for the chemotaxis assay as previously described by Liang *et al.*[21] It was found that SDF-1α induced a four-fold increase in the migration efficiency of E6-1 cells compared to the original Jurkat cells (Fig. 1b). Therefore, we decided to use E6-1 cells for the subsequent experiments.

Next, we attempted to optimize the experimental conditions for the SDF-1α-mediated chemotaxis assay. The chemotaxis index plateaued at approximately 60% after 3 h incubation of E6-1 cells with 400 ng/mL of SDF-1α (data not shown). We then examined the effect of increasing concentration of SDF-1α on the chemotaxis index and found that the level of chemotaxis was augmented in a dose-dependent manner and plateaued when more than 40 ng/mL of SDF-1α was used (Fig. 1c). Accordingly, the optimal condition for the chemotaxis assay in subsequent experiments was 100 ng/mL of SDF-1α for a 3h incubation period.

Next, we analyzed the cytotoxicity of CXCR4 antagonists to E6-1 cells. As indicated in Figure 2(a), the CXCR4 antagonists were not cytotoxic for E6-1 cells at a 10 μM concentration. To ascertain the possibility of these antagonists also exhibiting agonistic activities, we examined the chemotaxis activity of the antagonists. We observed that 100 ng/mL SDF-1α efficiently induced migration of E6-1; however, none of antagonists induced migration even at 10 μM (Fig. 2b). This indicated that the CXCR4 antagonists did not possess agonistic properties.

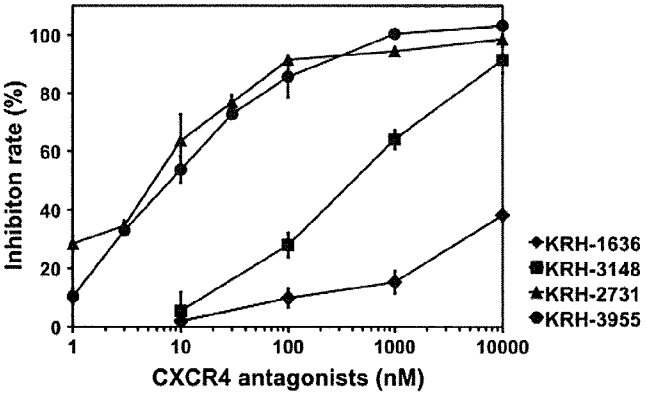


Fig. 3. Dose-dependent effect of CXC chemokine receptor-4 (CXCR4) antagonists on inhibition of stromal cell-derived factor-1α (SDF-1α)-mediated chemotaxis. E6-1 cells were pretreated with each concentration of CXCR4 antagonists at 37°C for 1 h, followed by incubation with 100 ng/mL of SDF-1α for 3 h. The cells were evaluated for the chemotaxis index. The inhibition rate was calculated as the percentage inhibition of chemotaxis by the antagonists.

**Table 1. Inhibitory effects of CXCR4 antagonists on SDF-1α-mediated chemotaxis and HIV-1 infection**

| CXCR4 antagonists | CXCR4 ($EC_{50}$, nM) | |
|---|---|---|
| | Chemotaxis | HIV-1 |
| KRH-1636 | >10 000 | 42 |
| KRH-3148 | 396.7 | 4 |
| KRH-2731 | 9.2 | 0.9 |
| KRH-3955 | 5.3 | 1 |

The effect of CXCR4 antagonists on the chemotaxis was investigated under the same conditions as described above. The prototype antagonist KRH-1636 inhibited the SDF-1α-mediated chemotaxis up to approximately 40% at a maximal concentration (10 μM). By contrast, KRH-3148 almost completely inhibited the chemotaxis at the maximal concentration; moreover, KRH-2731 and KRH-3955 showed the maximum inhibition rate even at 1 μM (Fig. 3). In order to quantitatively compare these efficacies, 50% effective concentration ($EC_{50}$) was calculated (Table 1). The results from this study clearly showed that KRH-2731 and KRH-3955 were effective at >1000-fold as compared with KRH-1636.

We further evaluated the effect of the compounds on HIV-1 infection. Anti-HIV-1 activities in nM of KRH-1636, KRH-3148, KRH-2731, and KRH-3955, which were shown as $EC_{50}$, were 42, 4, 0.9, and 1, respectively (Table 1). The efficacy of the antagonists was highly correlated with their inhibitory effects on HIV-1 infection by interrupting the association of the Env with CXCR4. Interestingly, inhibition of chemotaxis by KRH-1636 and KRH-3148 was relatively lower than that of HIV-1 infection compared with KRH-2731 and KRH-3955. The difference may be because action sites of KRH-2731 or KRH-3955 against CXCR4 are somewhat different from those of KRH-3148 (Sei Kumakura, unpublished data). In summary, these results demonstrate that both KRH-2731 and KRH-3955 are capable of efficiently inhibiting SDF-1α-mediated chemotaxis as well as infection of T cell–tropic HIV-1.

## Discussion

The present study demonstrated that the novel CXCR4 antagonists efficiently inhibited SDF-1α-mediated chemotaxis as well as


doi: 10.1111/j.1349-7006.2009.01104.x

infection of T cell-tropic HIV-1. Two compounds KRH-2731 and KRH-3955 were found to be highly potent inhibitors for both efficacies without any cytotoxicity or agonistic activity, indicating that they may be promising as anti-cancer metastasis and anti-HIV-1 drugs. In particular, both KRH-2731 and KRH-3955 efficiently inhibited calcium signaling induced by SDF-1α at a concentration of 10 nM, while KRH-3148 and KRH-1636 inhibited at 100 nM and at greater than 10 μM, respectively (Sei Kumakura *et al.*, unpublished results). This indicated that their antagonistic effects were highly correlated with their abilities to inhibit chemotaxis and HIV-1 infection.

While the Jurkat cell line expressed a smaller but almost comparable level of CXCR4 compared with E6-1 cells (Fig. 1a), their migration levels in the presence of SDF-1α were quite different (Fig. 1b). It is possible that the original Jurkat cells express non-functional CXCR4 with regard to signal transduction that is required for chemotaxis.

Tumor cells from various types of human cancers of epithelial, mesenchymal, and hematopoietic origins express high levels of CXCR4.[14,16] The interaction of SDF-1α with its receptor CXCR4 contributes to metastasis of breast cancer as well as a number of other malignancies in the lung, brain, and prostate. Furthermore, patients with cancers expressing high levels of CXCR4 have more extensive metastasis at lymph nodes compared with low CXCR4-expressing ones.[22] On this basis, the efficient CXCR4 antagonists demonstrated in this study may be highly valuable for the regulation of cancer metastasis. In fact, a synthetic peptide against CXCR4 efficiently inhibited metastasis of breast cancer in a mouse model,[21] thus providing support to our notion. However, a hurdle remains for the delivery of the peptide inihibitor to the primary focus of cancer in patients, thus impeding the clinical application of the inhibitor. In this regard, our low molecular weight CXCR4 antagonists are promising because they are non-cytotoxic and can be administered orally. In fact, KRH-3955 showed oral bioavailability of 25.6% in rats and its oral administration blocked X4 HIV-1 replication in the human peripheral blood lymphocytes and in severe combined immunodeficiency mouse system (Tsutomu Murakami *et al.*, manuscript in preparation). It is notable that AMD3100, another small non-peptide CXCR4 antagonist, has been shown to inhibit metastasis of cancer cells *in vitro* and *in vivo*.[23,24] Moreover, our preliminary data suggested that injection of the breast cancer cell line MDA-231 produced a huge tumor at the inoculated site as well as aggressive metastasis in the lungs of mice, and that our compounds partially inhibited both the primary tumor growth and the metastasis (data not shown).

In conclusion, CXCR4 antagonists, which can be orally administered, are promising agents for SDF-1α-mediated metastasis of cancer cells and also for the treatment and prophylaxis of a number of diseases related to the interaction between CXCR4 and SDF-1α, the best example of which would be an anti-HIV-1 drug.

## Acknowledgments

We thank M. Kannagi and S. Yamaoka, Tokyo Medical and Dental University, for critical discussions. This work was supported by grants from the Ministry of Education, Culture, Sports, Science and Technology; the Ministry of Health, Labor and Welfare; and Human Health Science of Japan.

## References

1 Ward SG, Westwick J. Chemokines: understanding their role in T-lymphocyte biology. *Biochem J* 1998; **333**: 457 70.
2 Le Y, Zhou Y, Iribarren P *et al.* Chemokines and chemokine receptors: their manifold roles in homeostasis and disease. *Cell Mol Immunol* 2004; **1**: 95–104.
3 Burger JA, Kipps TJ. CXCR4: a key receptor in the cross-talk between tumor cells and their microenvironment. *Blood* 2006; **107**: 1761–7.
4 Horuk R. Chemokine receptors. *Cytokine Growth Factor Rev* 2001; **12**: 313–15.
5 Nagasawa T, Hirota S, Tachibana K *et al.* Defects of B-cell lymphopoiesis and bone-marrow myelopoiesis in mice lacking the CXC chemokine PBSF/SDF-1. *Nature* 1996; **382**: 635–8.
6 Tachibana K, Hirota S, Iizasa H *et al.* The chemokine receptor CXCR4 is essential for vascularization of the gastrointestinal tract. *Nature* 1998; **393**: 591–4.
7 Zou YR, Kottmann AH, Kuroda M *et al.* Function of the chemokine receptor CXCR4 in haematopoiesis and in cerebellar development. *Nature* 1998; **393**: 595–9.
8 Burns JM, Summers BC, Wang Y *et al.* A novel chemokine receptor for SDF-1 and I-TAC involved in cell survival, cell adhesion, and tumor development. *J Exp Med* 2006; **203**: 2201–13.
9 Berger EA, Murphy PM, Farber JM. Chemokine receptors as HIV-1 coreceptors: roles in viral entry, tropism, and disease. *Annu Rev Immunol* 1999; **17**: 657–700.
10 Su L, Kaneshima H, Bonyhadi M *et al.* HIV-1-induced thymocyte depletion is associated with indirect cytopathogenicity and infection of progenitor cells in vivo. *Immunity* 1995; **2**: 25–36.
11 Bleul CC, Farzan M, Choe H *et al.* The lymphocyte chemoattractant SDF-1 is a ligand for LESTR/fusin and blocks HIV-1 entry. *Nature* 1996; **382**: 829–33.
12 Alkhatib G, Combadiere C, Broder CC *et al.* CC CKR5: a RANTES, MIP-1 alpha, MIP-1bata receptor as a fusion cofactor for macrophage-tropic HIV-1. *Science* 1996; **272**: 1955–8.
13 Cocchi F, DeVico AL, Garzino-Demo A *et al.* Identification of RANTES, MIP-1 alpha, and MIP-1 beta as the major HIV-suppressive factors produced by $CD8^+$ T cells. *Science* 1995; **270**: 1811–15.
14 Balkwill F. Cancer and the chemokine network. *Nature Rev Cancer* 2004; **4**: 540–50.
15 Luker KE, Luker GD. Functions of CXCL12 and CXCR4 in breast cancer. *Cancer Lett* 2006; **238**: 30–41.
16 Muller A, Homey B, Soto H *et al.* Involvement of chemokine receptors in breast cancer metastasis. *Nature* 2001; **410**: 50–6.
17 Liotta LA. An attractive force in metastasis. *Nature* 2001; **410**: 24–5.
18 Santiago B, Baleux F, Palao G *et al.* CXCL12 is displayed by rheumatoid endothelial cells through its base amino-terminal motif on heparan sulfate proteoglycans. *Arthritis Res Ther* 2006; **8**: R43.
19 Ichiyama K, Yokoyama-Kumakura S, Tanaka Y *et al.* A duodenally absorbable CXC chemokine receptor 4 antagonist, KRH-1636, exhibits a potent and selective anti-HIV-1 activity. *Proc Natl Acad Sci USA* 2003; **100**: 4185–90.
20 Tamamura H, Hori A, Kanzaki N *et al.* T140 analogs as CXCR4 antagonists identified as anti-metastatic agents in the treatment of breast cancer. *FEBS Lett* 2003; **550**: 79–83.
21 Liang Z, Wu T, Lou H *et al.* Inhibition of breast cancer metastasis by selective synthetic polypeptide against CXCR4. *Cancer Res* 2004; **64**: 4302–8.
22 Dewan MZ, Ahmed S, Iwasaki Y *et al.* Stromal cell-derived factor-1 and CXCR4 receptor interaction in tumor growth and metastasis of breast cancer. *Biomed Pharmacother* 2006; **60**: 273–6.
23 Yoon Y, Liang Z, Zhang X *et al.* CXC chemokine receptor-4 antagonist blocks both growth of primary tumor and metastasis of head and neck cancer in xenograft mouse models. *Cancer Res* 2007; **67**: 7518–24.
24 Li JK, Yu L, Shen Y *et al.* Inhibition of CXCR4 activity with AMD3100 decreases invasion of human colorectal cancer cells *in vitro*. *World J Gastroenterol* 2008; **14**: 2308–13.

Journal of Cellular Physiology



# Dys-Regulated Activation of a Src Tyroine Kinase Hck at the Golgi Disturbs *N*-Glycosylation of a Cytokine Receptor Fms

RANYA HASSAN,[1] SHINYA SUZU,[1] MASATERU HIYOSHI,[1] NAOKO TAKAHASHI-MAKISE,[1] TAKAMASA UENO,[2] TSUTOMU AGATSUMA,[3] HIROFUMI AKARI,[4] JUN KOMANO,[5] YUTAKA TAKEBE,[6] KAZUO MOTOYOSHI,[7] AND SEIJI OKADA[1]*

[1]*Division of Hematopoiesis, Center for AIDS Research, Kumamoto University, Kumamoto, Kumamoto, Japan*

[2]*Viral Immunology, Center for AIDS Research, Kumamoto University, Kumamoto, Kumamoto, Japan*

[3]*Tokyo Research Laboratories, Kyowa Hakko Co., Ltd, Machida, Tokyo, Japan*

[4]*Laboratory of Disease Control, Tsukuba Primate Research Center, National Institute of Biomedical Innovation, Tsukuba, Ibaraki, Japan*

[5]*Laboratory of Virology and Pathogenesis, AIDS Research Center, National Institute of Infectious Diseases, Shinjuku, Tokyo, Japan*

[6]*Laboratory of Molecular Biology and Epidemiology, AIDS Research Center, National Institute of Infectious Diseases, Shinjuku, Tokyo, Japan*

[7]*Department of Internal Medicine, National Defense Medical College, Tokorozawa, Saitama, Japan*

HIV-1 Nef accelerates the progression to AIDS by binding with and activating a Src kinase Hck, but underlying molecular basis is not understood. We revealed that Nef disturbed *N*-glycosylation/trafficking of a cytokine receptor Fms in an Hck-dependent manner, a possible trigger to worsen uncontrolled immune system. Here, we provide direct evidence that dys-regulated activation of Hck pre-localized to the Golgi apparatus causes this Fms maturation arrest. A striking change in Hck induced by Nef other than activation was its skewed localization to the Golgi due to predominant Golgi-localization of Nef. Studies with different Nef alleles and their mutants showed a clear correlation among higher Nef-Hck affinity, stronger Hck activation, severe Golgi-localization of Hck and severe Fms maturation arrest. Studies with a newly discovered Nef-Hck binding blocker 2c more clearly showed that skewed Golgi-localization of active Hck was indeed the cause of Fms maturation arrest. 2c blocked Nef-induced skewed Golgi-localization of an active form of Hck (Hck-P2A) and Fms maturation arrest by Nef/Hck-P2A, but showed no inhibition on Hck-P2A kinase activity. Our finding establishes an intriguing link between the pathogenesis of Nef and a newly emerging concept that the Golgi-localized Src kinases regulate the Golgi function.

J. Cell. Physiol. 221: 458–468, 2009. 

Studies of HIV-1-infected patients and monkey models have demonstrated that Nef, a protein with no enzymatic activity encoded by the HIV-1 genome, is a critical determinant for the development of AIDS (Kestler et al., 1991; Deacon et al., 1995; Kirchhoff et al., 1995). Subsequent studies of HIV-1 transgenic (Tg) mice supported the idea. The expression of entire coding sequences of HIV-1 in $CD4^+$ T cells and macrophages caused an AIDS-like disease, which was abolished by Nef deletion (Hanna et al., 1998). This pathogenetic activity of Nef is supposed to be mediated by its binding with cellular proteins, and a well-defined partner of Nef is Hck (Saksela et al., 1995), a member of Src family tyrosine kinases expressed in macrophages. Other Src kinases (Lyn, Fyn, c-Src, and Lck) bind Nef but with lower affinities (Arold et al., 1998; Karkkainen et al., 2006; Trible et al., 2006). Importantly, the disruption of proline-rich PxxP motif of Nef, an essential motif to bind the Src homology 3 (SH3) domain of Hck, was sufficient to protect Tg mice from the AIDS-like disease, and wild-type Nef-induced disease progression was significantly delayed in $Hck^{-/-}$ mice (Hanna et al., 2001), indicating that high affinity Nef-Hck binding in macrophages is at least in part responsible for disease development and progression. However, unresolved issue is how Nef-Hck binding followed by activation of Hck (Moarefi et al., 1997; Lerner and Smithgall, 2002) satisfactorily account for disease development and progression.

An important clue to the issue is that Nef predominantly localized to the Golgi apparatus (Greenberg et al., 1998; Drakesmith et al., 2005; Haller et al., 2007) and that Nef not only activated Hck but also induced skewed localization of Hck to the Golgi (Hung et al., 2007). The Golgi functions as a sorting hub and location of glycosylation for proteins, and several lines of evidence have revealed that Src kinases, shown to be involved in a wide array of intracellular signaling (reviewed in

Contract grant sponsor: Ministry of Education, Culture, Sports, Science and Technology of Japan.
Contract grant sponsor: Human Science Foundation, Japan.

*Correspondence to: Seiji Okada, Division of Hematopoiesis, Center for AIDS Research, Kumamoto University, Kumamoto 860-0811, Japan. E-mail: okadas@kumamoto-u.ac.jp

Received 17 February 2009; Accepted 11 June 2009

Published online in Wiley InterScience (www.interscience.wiley.com.), 7 July 2009.
DOI: 10.1002/jcp.21878

Lowell, 2004), also play a role in the regulation of the Golgi structure/function. First, a fraction of Src kinases, including Hck, is physiologically found at the Golgi (David-Pfeuty and Nouvian-Dooghe, 1990; Kaplan et al., 1992; Ley et al., 1994; Bijlmakers et al., 1997; van't Hof and Resh, 1997; Carreno et al., 2000; Kasahara et al., 2004). Second, fibroblasts lacking three ubiquitous Src kinases (c-Src/Yes/Fyn) exhibited an aberrant Golgi structure composed of collapsed stacks and bloated cisternae (Bard et al., 2003). Third, an increased protein load entering the *cis*-Golgi from the endoplasmic reticulum activated the Golgi-localized Src kinases, which in turn regulated overall protein trafficking activity in the secretory pathway (Pulvirenti et al., 2008). Importantly, the study by Pulvirenti et al. indicates that coordinated regulation of activity of the Golgi-localized Src kinases is crucial to maintain the Golgi function, which raises an intriguing possibility that Nef affects protein trafficking process and thereby macrophage phenotype/function through skewed Golgi-localization of active Hck.

Indeed, we recently identified an aberrant function of Nef, which was possibly due to the skewed Golgi-localization of active Hck. We previously found that Nef inhibited the signal of M-CSF, a primary cytokine for macrophages (Suzu et al., 2005), which was a possible trigger to worsen uncontrolled immune systems in patients, as M-CSF is essential to maintain macrophages at an anti-inflammatory state (reviewed in Hamilton, 2008). Of interest was the role of Hck in this inhibitory activity of Nef (Hiyoshi et al., 2008). Nef reduced cell surface expression of M-CSF receptor Fms in myeloid cells and macrophages, which was the direct cause of the inhibitory activity of Nef on M-CSF signal. Importantly, such reduced cell surface expression of Fms was reproduced in transfected 293 cells, but only in co-expression with Hck. More importantly, the reduced cell surface expression was due to the accumulation of an immature under-*N*-glycosylated Fms at the Golgi (hereinafter called Fms maturation arrest). However, constitutive-active Hck alone failed to induce such Fms maturation arrest. These results indicate that Nef inhibits M-CSF signal by arresting Fms *N*-glycosylation and trafficking at the Golgi and that such Fms maturation arrest was not caused just because of Hck activation. Thus, a most likely cause of Nef-induced Fms maturation arrest was skewed Golgi-localization of active Hck. However, this intriguing hypothesis should be carefully and directly tested, because it will not only help to clarify molecular basis of this novel function of Nef through Hck, but also provide an excellent example of disease-associated failure of the Golgi function regulation by the Golgi-localized Src kinases.

In this study, we therefore sought to definitely conclude that skewed Golgi-localization of active Hck was indeed the direct cause of Fms maturation arrest by Nef. To this end, we employed two different approaches. First, we prepared various Nef proteins and compared their abilities to induce skewed Golgi-localization of Hck, Hck activation and Fms maturation arrest. Second and importantly, we discovered a small-molecule non-kinase inhibitor that effectively blocked Nef-Hck binding and performed mechanistic analyses with the newly discovered compound.

## Materials and Methods

### Expression plasmids

For the expression in HEK293 cells (Invitrogen, Carlsbad, CA), human Fms- and human p56Hck cDNA cloned into pCDNA3.1 vector (Invitrogen) were used (Suzu et al., 2005; Hiyoshi et al., 2008). The constitutive-active Hck P2A mutant (Hiyoshi et al., 2008) was also used in selected experiments. The expression plasmid for human Lyn cloned in pME-puro vector was provided by Y. Yamanashi (Tokyo Medical and Dental University, Tokyo, Japan) and used in the pull-down assay with GST-Nef fusion proteins (see below). Nef cDNA derived from the NL43 or SF2 strain of HIV-1 was cloned into pRc/CMV-CD8 vector to express the extracellular/transmembrane regions of CD8-Nef fusion protein (Hiyoshi et al., 2008). NL43 Nef-M20A was prepared as described previously (Akari et al., 2000). NL43 Nef-AxxA and $-\Delta E$ mutant were provided by A. Adachi (University of Tokushima, Tokushima, Japan) and J.C. Guatelli (University of California, San Diego, CA), respectively. In this study, we prepared another NL43 Nef mutant (NL43 Nef-TR), by using QuikChange II Site-directed Mutagenesis Kits (Stratagene, La Jolla, CA). We also prepared Nef constructs expressing Nef-GFP fusion proteins (Ueno et al., 2008). For the expression of GST-Nef fusion proteins, fragments containing the entire coding sequences of the wild-type NL43 Nef, NL43 Nef-TR mutant, wild-type SF2 Nef, and SF2 Nef-AxxA mutant were subcloned into pGEX-6P-1 vector (GE Healthcare, Buckinghamshire, UK). SF2 Nef-AxxA mutant was prepared by using QuikChange II Site-directed Mutagenesis Kits (Stratagene). The nucleotide sequences of the coding region of all Nef constructs were verified by using BigDye Terminator v3.1 Cycle Sequencing Kit (Applied Biosystems, Foster City, CA) and ABI PRISM 3100 Genetic Analyzer (Applied Biosystems).

### Chemicals

PP2 (Sigma, San Diego, CA) was used as the Src kinase inhibitor. UCS15A and its synthetic derivatives, 2b and 2c, were prepared as described (Oneyama et al., 2003). All these inhibitors were dissolved in dimethyl sulfoxide (DMSO; Wako, Osaka, Japan).

### Western blotting

HEK293 cells were maintained with DME medium (Wako) supplemented with 10% fetal calf serum (FCS). The maturation of Fms proteins or the activation of Hck was analyzed by the transient expression assay with the cells followed by Western blotting as described previously (Suzu et al., 2005; Hiyoshi et al., 2008). In brief, cells grown on a 12-well tissue culture plate were transfected with plasmid for Fms (0.4 μg), Nef (0.8 μg), or Hck (0.4 μg) in the combinations indicated using LipofectAMINE2000 reagent (Invitrogen), unless otherwise stated. Total amounts of plasmids were normalized with the empty vectors. After 6 h, culture medium was replaced with complete medium and the transfected cells were cultured for an additional 42 h. In selected experiments, chemicals such as PP2 and 2c were added to the culture at the same time of changing medium. Total cell lysates were prepared essentially as described (Suzu et al., 2000). Primary antibodies used for Western blotting were as follows: anti-Fms (C-20; Santa Cruz Biotechnology, Santa Cruz, CA), anti-CD8 (H-160; Santa Cruz), anti-GFP (FL; Santa Cruz), anti-Hck (clone 18; Transduction Laboratories, Lexington, KY), anti-Hck phosphorylated at tyrosine 411 (Hck-pTyr$^{411}$; Santa Cruz), anti-phosphotyrosine (PY99; Santa Cruz), and anti-ERK1/2 (K-23; Santa Cruz). The relative intensity of bands on scanned gel images was quantified using NIH Image software, and the Fms maturation arrest or Hck activation is also shown graphically on an arbitrary unit. The relative intensity of bands on Hck-pTyr$^{411}$ blots was quantified and the degree of Hck activation was expressed as a fold-increase relative to the control. For Fms maturation arrest, we calculated the percentage of immature under-*N*-glycosylated Fms of total Fms protein amount, and compared the percentages among samples.

### Immunofluorescence

The signal of Nef-GFP was directly visualized with a BZ-8000 fluorescent microscope (Keyence, Osaka, Japan) equipped with Plan-Fluor ELWD 20x/0.45 objective lenses (Nikon, Tokyo, Japan) (Hiyoshi et al., 2008). To detect active Hck, cells were fixed in 2% paraformaldehyde, permeabilized with ethanol, and stained with goat anti-active Hck antibodies (Santa Cruz). Secondary antibodies were anti-goat IgG-AlexaFluo488 (Molecular Probes, Eugene, OR). Nuclei were stained with DAPI (Molecular Probes), and

fluorescent signals were visualized as above. Image processing was performed using BZ-analyzer (Keyence) and Adobe Photoshop Software (Adobe Systems, San Jose, CA).

### GST pull-down

The control GST or GST-Nef fusion proteins (wild-type NL43 Nef, NL43 Nef-TR, wild-type SF2 Nef, and SF2 Nef-AxxA) cloned in pGEX-6P-1 vector was expressed in *E. coli* BL21 cells (GE Healthcare). Cells were grown in LB media containing 50 μg/ml ampicillin followed by induction with 1 μM IPTG. The expression-induced cells were harvested and lysed with BugBuster Protein Extraction Reagent containing 1 U/ml rLysozyme and 25 U/ml Benzonaze Nuclease (Novagen, Madison, WI). The cleared lysates were then incubated with GST-Bind Resin (Novagen). After extensive washing with GST Bind/Wash Buffer (Novagen), the resin was incubated with the total cell lysates of HEK293 cells transfected with the expression plasmid for Hck or Lyn. In a selected experiment, 2c was added to the mixtures. After extensive re-washing, the resin was boiled with SDS–PAGE sample buffer and elutes were analyzed for the presence of Hck or Lyn by western blotting. Primary antibodies used were as follows (both from Transduction Laboratories): anti-Hck (clone 18) and anti-Lyn (clone 42). In a selected experiment, we also used GST proteins fused to the SH3 domain of Hck (Paliwal et al., 2007), which was provided by G. Swarup (Center for Cellular and Molecular Biology, Hyderabad, India).

### Subcellular fractionation

The subcellular fractionation on sucrose gradients was performed exactly as reported (Matsuda et al., 2006). In brief, cells were

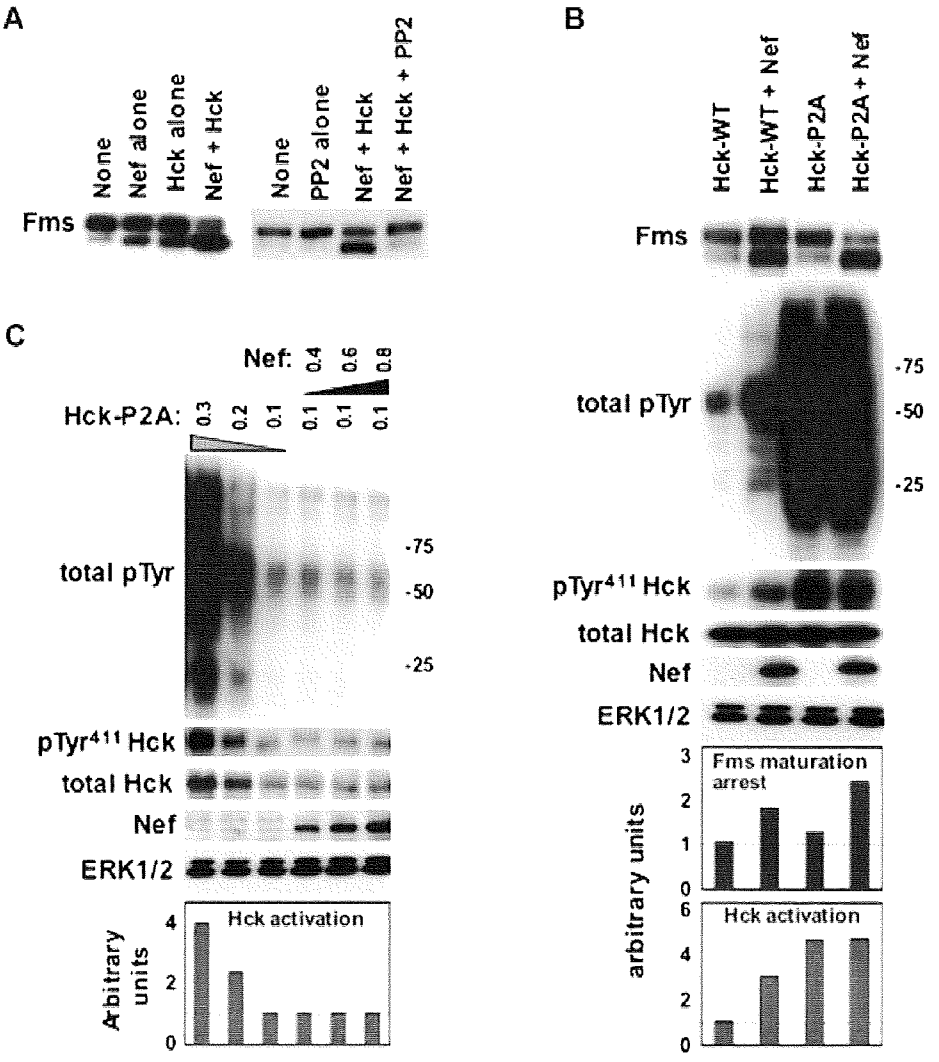


**Fig. 1. Nef/Hck-induced Fms mturation arrest. A: HEK293 cells were transfected with Fms plamid alone (None) or co-transfected with the plasmids for NL43 Nef and/or wild-type Hck as indicated. In the right blot, PP2 was added to selected wells at a final concentration of 10 μM after the transfection, Total cell lysates were subjected to Fms Western blotting. B: Cells were transfected with Fms plasmid alone (None) or in combination with the plasmids for Nef (NL43) and Hck (WT or constitutive-active P2A), as indicated. These cells were then analyzed for the expression of Fms, tyrosine-phosphorylated proteins (total pTyr), active-Hck (pTyr$^{411}$Hck), total Hck, CD8-Nef (Nef), or ERK by Western blotting. The ERK blot is a loading control. The quantified Fms maturation arrest and Hck activation are shown in the bar graphs. C: Cells were transfected with varying amounts (μg) of Hck-P2A and NL43 Nef plasmids as indicated, and analyzed as in (B). The quantified Hck activation is shown in the bar graphs. [Color figure can be viewed in the online issue, which is available at www.interscience.wiley.com.]**